Methane + Propane Mixed Gas Hydrate Studies Using the 3-in-1 Technique

Études d'Hydrates de Gaz d'un Mélange de Méthane + Propane en Utilisant la Technique 3-en-1

A Thesis Submitted to the Division of Graduate Studies
of the Royal Military College of Canada
by

Sebastián Camilo Ovalle

In partial Fulfillment of the Requirements for the Degree of
Master of Applied Science

December, 2019

To my mother, Constanza, for her unfathomable love, selfless sacrifice, and relentless support, and hoping to be worthy of all her efforts someday. To my family, for casting their light on my way although far away. To my supervisor Dr. Juan Beltran, my deepest gratitude for his trust, patience, encouragement, and especially for so many life lessons I learned from him. You are the best and only true mentor I ever had. *Festina lente*. To Andrés, Camilo, Daniel, and Jorge, for their sincere friendship and support. To Nestor, for teaching me that "this is worth it" and not to give up in the face of adversity. To my Kingstonian family, for always making me feel at home.

Acknowledgements

The financial support from the Natural Sciences and Engineering Research Council of Canada (NSERC), the Canadian Foundation for Innovation (CFI), and the Royal Military College of Canada Short Term Research Needs Program is greatly appreciated. I am deeply thankful to Fundación Hogar and its president Luz María de Mendez, for their valuable support that made my master's possible. And last but not least, to Margarita de Medina, whose immense heart never ceases to amaze me. I will forever be in debt for your sincere help and trust, and I hope to be of service to my fellow human beings the way you have always done it.

Abstract

The 3-in-1 technique was applied to hydrates of binary mixtures of methane + propane (90:10 and 98:2 mole ratios). Hydrate morphology showed a strong dependence on subcooling. Three groups of crystal habits were identified: below 1.5 K subcooling, the dominant habit was elongated polyhedral crystals; between subcoolings of 2.0 to 3.0 K, a granular habit dominated the morphology, with more rounded polyhedral crystals embedded in the crystal film. Towards 3.5 K and higher subcoolings, the hydrate film was smoother, and individual granules became indistinguishable. Single polyhedral crystals within the film were smaller, and indistinguishable at subcoolings higher than 5.0 K. These differences in morphology suggest growth mechanisms strongly dependent on driving force. The habit of single crystals closely resembled that of the film, but their morphologies diverged with increasing subcooling. Individual crystals sometimes detached from the main film and grew independently and with different morphologies than that of the film. Conversely, single crystals that had grown independently from the main film attached to and assumed the film morphology. These observations suggest at least two growth mechanisms could present at once during hydrate growth. Regardless of driving force, growing crystals were observed to partially dissociate and reform as the clathrate film grew. This phenomenon could be due to instability of some crystals that transform into their most stable form. Another explanation could be local gradients of guest concentration in the liquid phase that could cause the dissociation. Hydrate-liquid-vapor equilibrium temperatures were measured with minimum uncertainties and agreed with those reported in literature for the studied systems. Growth rates showed a strong dependence on subcooling and could be measured under several degrees of subcooling with a single gradient experiment. Growth rates of single crystals and the hydrate film were similar at lower driving forces and diverged when subcooling was higher than 2.5 K. These differences in growth rates provide evidence of the onset of different mechanisms and could explain the observed changes in crystal habit with driving force. The 3-in-1 technique was shown to be a precise, multifaceted tool to evaluate hydrates from binary gas mixtures, that provides visual evidence of complex crystal growth mechanisms occurring during their crystallization.

Résumé

La technique 3-en-1 a été appliqée aux hydrates de mélanges binaires de méthane + propane (rapports molaires 90:10 et 98:2). La morphologie des hydrates présente une forte dépendance au sous-refroidissement. Trois groupes d'habitus cristallin ont été identifiés : en dessous de 1.5 K, l'habitus était dominée par des cristaux polyédriques allongés ; Entre les sous-refroidissements de 2.0 à 3.0 K, un habitus granulaire dominait la morphologie, avec des cristaux polyédriques plus arrondis noyés dans le film cristallin. Vers 3.5 K et plus de sous-refroidissement, le film d'hydrate était plus lisse et les granules individuels devenaient indiscernables. Les cristaux simples polyhèdraux dans le film étaient plus petits et impossibles à distinguer aux sous-refroidissements supérieurs à 5.0 K. Ces différences de morphologie suggèrent des mécanismes de croissance fortement dépendants de la force motrice. L'habitus des mono-cristaux ressemblait beaucoup à celle du film, mais leurs morphologies divergeaient avec l'augmentation du sous-refroidissement. On a observé que les cristaux se détachent du film et se développent en différentes morphologies. Inversement, certains mono-cristaux sont fixés au film d'hydrate et se développent dans la morphologie du film. Ces observations suggèrent qu'au moins deux mécanismes de croissance pourraient se présenter simultanément lors de la croissance des hydrates. Indépendamment de la force motrice, on a observé que les cristaux en croissance se dissociaient et se reformaient constamment à mesure que le film de clathrate se développait. Ce phénomène pourrait être dû à l'instabilité de certains cristaux qui se transforment en leur forme la plus stable. Une autre explication pourrait être les gradients locaux de concentration dans la phase liquide qui pourraient provoquer la dissociation. Les températures d'équilibre hydrate-liquide-vapeur ont été mesurées avec un minimum d'incertitudes et conformes à celles rapportées dans la littérature pour les systèmes étudiés. Les taux de croissance montraient une forte dépendance vis-à-vis du sous-refroidissement et pouvaient être mesurés sous plusieurs degrés de sous-refroidissement avec des expériences à un seul gradient. Les taux de croissance des monocristaux et du film d'hydrate sont similaires lorsque les forces motrices sont faibles et divergent lorsque le sous-refroidissement est supérieur à 2.5 K. Ces différences dans les taux de croissance témoignent de l'apparition de mécanismes différents et pourraient expliquer les changements observés dans le comportement cristallin avec la force motrice. La technique 3-en-1 s'est révélée être un outil précis et multiforme permettant d'évaluer les hydrates issus de mélanges de gaz binaires et de fournir une preuve visuelle des mécanismes complexes de croissance des cristaux se produisant pendant leur cristallisation.

Contents

List of Figures

List of Tables

Nomenclature

k	Boltzmann constant
μ	Chemical potential
y	Gas mole fraction
H	Hydrate phase
v	Hydrate-film-growth velocity
n	Hydration number
x	Liquid mole fraction
L	Liquid phase
P	Pressure
u	Standard uncertainty
T	Temperature
V	Vapor phase

Superscripts/Subscripts

h	High-temperature side of the stage
HLV	Hydrate-Liquid Water-Vapor
c	Low-temperature side of the stage
sub	Subcooling

Chapter 1

Introduction

Clathrate hydrates, also known as gas hydrates, are crystalline, non- stoichiometric compounds formed when small molecules (guest) are trapped within a lattice of hydrogen-bonded cages of "host" molecules (Sloan, 2004). Hydrates are usually found in nature when different light hydrocarbons, such as methane, propane, and ethane, are encapsulated within water cages, forming a solid solution (Englezos, 1993).

Hydrates have stirred curiosity among researchers since Sir Humphry Davy discovered them in 1810 (Davy, 1811). In 1934, when Hammerschmidt (1934) confirmed that hydrates were responsible for plugging in oil and gas pipelines, interests moved toward techniques and additives for hydrate inhibition (Sloan and Koh, 2008b). The obstruction of pipelines is one of the major technical concerns for oil and gas companies, and flow assurance in this industry demands a high economic investment (Sloan, 2004).

It is estimated that gas hydrates in nature could store up to double the amount of energy as all other fossil fuels combined (Koh et al., 2011). In addition, the volumetric gas concentration in hydrates can be comparable to the energy density found in compressed natural gas (CNG) (Sloan, 2003). Since natural gas is a mixture of different gases, understanding the particular characteristics of hydrate formation and dissociation with hydrocarbon mixtures is necessary for the further development of hydrate-based technologies.

Characterization of hydrates typically requires several pieces of specialized equipment (Sloan and Koh, 2008b). However, DuQuensay et al. (2016) designed a reactor in which phase equilibrium, morphology, and kinetics, all critical properties of hydrates, could be measured with a single apparatus (3-in-1 technique). Studying each one of these characteristics with other techniques would require separate pieces of equipment, and experimental times in the order of hours and days. The 3-in-1 method has proven to significantly improve on those limitations (DuQuensay et al., 2016; Kumar et al., 2019).

The 3-in-1 technique has been used with methane and CO_2 and provided reproducible morphologies, hydrate-liquid-vapor equilibrium conditions, and film kinetics (Sandoval, 2015; DuQuensay et al., 2016). Some mixtures of methane + CO_2 were also evaluated using this technique (Ortiz, 2017). Hydrates formed with methane + propane mixtures have more complex growth mechanisms than single guests and resembles natural gas. Using the 3-in-1 technique to evaluate methane + propane mixtures is an important step towards characterizing natural gas systems with this versatile tool.

The objective of the present work is to evaluate the suitability of the 3-in-1 technique to study gas hydrate systems with binary mixtures of methane + propane. To do so, hydrate film growth kinetics, phase equilibria, and morphological features of methane + propane hydrates were measured. Additionally, mechanistic aspects of hydrate growth were studied, particularly growth mechanisms and polymorphism reported for these systems in the literature.

Chapter 2

Background

Gas hydrates are comprised of a small (<9 Å) guest molecule trapped inside a lattice of hydrogen-bonded cages of host molecules (Sun et al., 2010). Gas hydrates are usually formed at temperatures below 300 K and pressures above 0.6 MPa (Sloan, 2003).

After their discovery in 1810 by Sir Humphry Davy, who formed a solid solution of chlorine gas and water above the normal freezing temperature of water (Davy, 1811), interest in these compounds was kept between the boundaries of pure academic curiosity (Sloan and Koh, 2008b). In 1934 gas hydrates were identified as one cause of plugging in oil and gas pipelines (Hammerschmidt, 1934). Industrial concern led to developing multiple techniques to avoid hydrate plugging, including additives such as hydrate inhibitors (Kelland, 2006).

When *in situ* hydrates were discovered in 1965, renewed interest in these compounds arose from the possibility to use them as a new source of energy (Makogon, 1965). Conservative estimates of the total hydrate reserves in the world suggest that they could double the reserves of other fossil fuels combined (Sloan, 2003). Since methane has 21 times the greenhouse effect of carbon dioxide, (Sloan, 2004) decomposition of natural gas hydrates reserves could enhance the current trend of global warming (Englezos, 1993; Koh et al., 2011). Further research is necessary on technologies required for exploration and recovery, and also on the environmental impact of future use of natural gas hydrates (Englezos, 1993; Koh et al., 2011).

Among technologies that could emerge from hydrate research is the storage and transportation of natural gas in the form of hydrates (Koh et al., 2011). Since it has been estimated that 70% of the global gas reserves are either too far from existing pipelines or too small to economically justify other means of transportation (e.g., liquefaction facilities) hydrate technology research seems to be able to provide a different solution to this problem (Sloan, 2003). Other feasible technologies derived from hydrate research include separation technologies, especially

those too expensive or too difficult to perform by other means (Englezos, 1993); and sequestration of carbon dioxide either from flue gases or the atmosphere, to counteract the current climate change trends (Koh et al., 2011).

2.1 Clathrate Hydrates

Hydrates have a defined crystalline structure of hollow polyhedra, which act as hosts of guest molecules (Koh et al., 2011). Inclusion compounds are formed when two different molecular species are arranged as a cage and as a guest (Englezos, 1993). Depending on the nature of the host molecule, clathrates can also be divided into aqueous clathrates, in which the host molecule is water, and non-aqueous clathrates (Englezos, 1993). This work deals with aqueous clathrates, also referred to as gas hydrates or simply hydrates.

Since hydrates are usually made of 85% water molecules on a molar basis, they exhibit similar characteristics to ice, such as density, refractive index, and appearance, but differ with the latter in some other properties such as heat capacity, mechanical strength and thermal conductivity (Koh et al., 2011). It is known that guest molecules in hydrates could be concentrated by a factor up to 180 (Sloan et al., 2011). As an example, 1 m^3 of hydrate can host 163 m^3 of methane at 1 atm and 273 K (Sloan, 2004). The term "hydration number" (n) is used to describe the water-to-guest mole ratio. For methane hydrates it is usually $n = 6$ (Sloan and Koh, 2008a).

The three most common hydrate crystal structures are structure I (sI), structure II (sII), and structure H (sH) (Koh et al., 2011). Structures I and II are those commonly found in oil and gas production environments (Sloan and Koh, 2008b). The type of structure formed, as well as the formation pressure and temperature are usually determined by the guest-to-cage size ratio (Sloan et al., 2011).

2.1.1 Crystalline Structure

The simplest structure, structure I (sI), is comprised of two different cage types: a pentagonal dodecahedral (5^{12}) cage and a larger cage ($5^{12}6^2$), with 12 pentagonal and 2 hexagonal faces (Figure 2.1) (Koh et al., 2011).

The 5^{12} cage is the basic building block of the three mentioned structures, and the structure will be determined by the other cages stabilizing the 5^{12} (Sloan, 2003). For sII, the basic cage is stabilized with a larger cage ($5^{12}6^4$) and for sH with a $4^35^66^3$ cage of medium size and a larger $5^{12}6^8$ icosahedral cage (Figure 2.1) (Koh et al., 2011).

The size of the guest molecule usually defines the type of crystalline structure to be formed. For some molecules the cages of sI are too small, so they will tend to form crystal structures with larger cages, such as sII and sH (Sloan, 2003; Koh

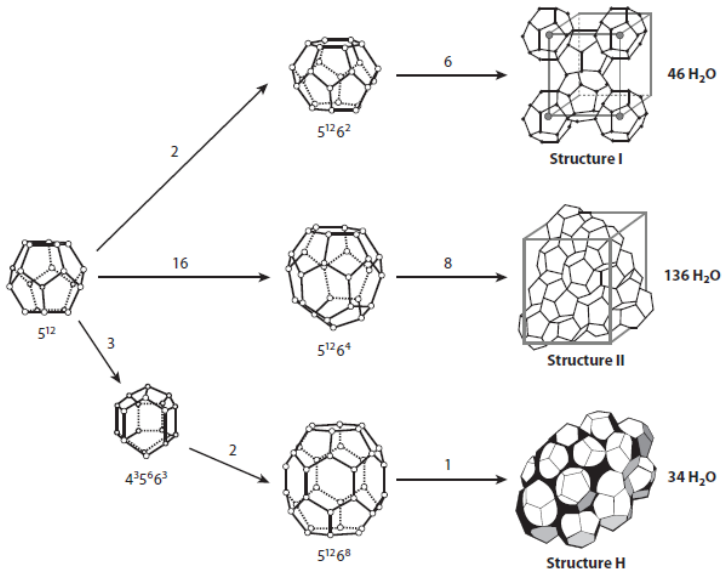

Figure 2.1: Common gas hydrates crystalline structures with their respective unit cages. Basic unit cage is a pentagonal dodecahedron (5^{12}). Republished with permission of Annual Reviews, Inc., from "Fundamentals and Applications of Gas Hydrates", Carolyn A. Koh, E. Dendy Sloan, Amadeu K. Sum, and David T. Wu, 2, 2011; permission conveyed through Copyright Clearance Center, Inc.

et al., 2011). In table 2.1 some guest molecules and the corresponding hydrate crystalline structures are presented.

2.1.1.1 Transformation

In a crystallization process, the first structure to grow is not necessarily the most stable, but the one leading to less change in free energy (Mullin, 2001). Therefore, crystals can transform into more stable structures, even in the solid phase. This phenomenon is known as the Ostwald step rule, and although there is not a definite thermodynamic explanation (Mullin, 2001), it has been shown to minimize the crystallization entropy production (Santen, 1984).

Transformations can occur when the already-formed crystals are brought to different thermodynamic conditions. This change can be observed as some crystals dissociate and recrystallize into their most stable forms (Schicks and Ripmeester, 2004; Schicks et al., 2006).

Table 2.1: Some gas guest molecules, their respective hydrate crystalline structures and equilibrium temperatures at atmospheric pressure. Modified from Sloan and Koh (2008a)

Guest Molecule	Structure	T_{HLV} [K], ($P = 1$ atm)
CO_2	I	218.15
H_2S	I	273.55
CH_4	I	195.15
C_2H_6	I	239.44
C_3H_8	II	261.55
iso-butane	II	270.35

2.2 Phase Equilibria

The number of independent, intensive variables that have to be specified to characterize phase equilibrium in a closed, non-reacting system is given by the Gibbs Phase Rule (Equation 2.1).

$$F = 2 + N - \pi \tag{2.1}$$

In Equation 2.1, F is the number of intensive variables (i.e., degrees of freedom), N is the number of components in the system, and π is the number of phases present (Smith et al., 2001). In the case of a single guest ($F = 1$), one intensive variable must be controlled, and another reported to justify equilibrium (Beltran et al., 2012). For single-guest systems, the hydrate-liquid-vapor (HLV) equilibrium can be represented in a PT phase diagram as a curve such as that in Figure 2.2. Above the HLV curve, hydrates will form and below they will dissociate. The curve in Figure 2.2 was obtained using CSMGem, a program developed at the Colorado School of Mines (Sloan and Koh, 2008a). CSMGem calculates hydrate-liquid-vapor equilibrium using Gibbs energy minimization.

For a binary mixture of hydrate formers ($F = 2$), two variables must be controlled and a third one reported. The HLV equilibrium, depicted as a curve for a single guest in Figure 2.2, would require a third axis with composition y_i and would be represented as a surface or a series of contour lines on a 2D PT diagram.

2.2.1 Mixtures of Hydrate Formers

Hydrates found in nature and industry are made of a mixture of different gases, usually light hydrocarbons and carbon dioxide. The presence of different guest molecules in the hydrate-forming mixture can lead to the formation of different

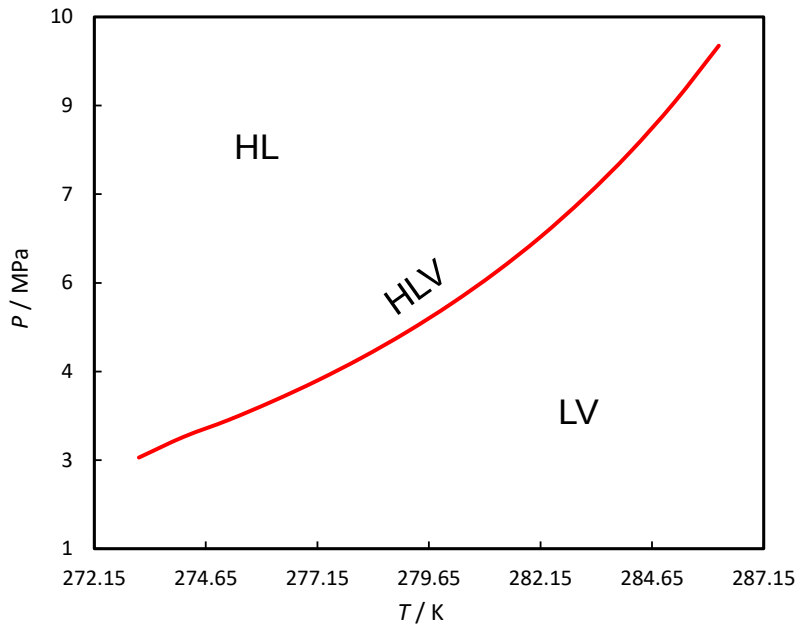

Figure 2.2: Calculated pressure-temperature partial phase diagram with three-phase equilibrium (HLV) curve for methane + water system (Sloan, 1998).

crystalline structures and the growth of two coexisting structures in the hydrate phase (Sloan and Koh, 2008b; Uchida et al., 2004).

Mixed hydrates can exhibit substantially different HLV equilibrium pressures than those of the pure guests at the same temperature. In the methane + propane system depicted in Figure 2.3 (green curve), predicted equilibrium pressure for pure methane at 274.2 K is over 2 times that of the system containing a mole fraction of only 2% propane. When the propane mole fraction is increased to 10% (Figure 2.3, purple curve), the equilibrium pressure at 274.2 K is 5 times lower than that of pure methane at the same temperature. This particular phenomenon could lead to hydrate formation at lower pressures and higher temperatures than those expected for pure systems.

Hydration rates can differ significantly between guests in a mixture. Therefore the gas phase can drastically change its composition if the hydrate grows in a water-dominated system (Sloan and Koh, 2008b). If the partial pressure of the remaining guest is reduced below its equilibrium pressure after the first formation, no more hydrate growth should be observed afterwards (Uchida et al., 2004).

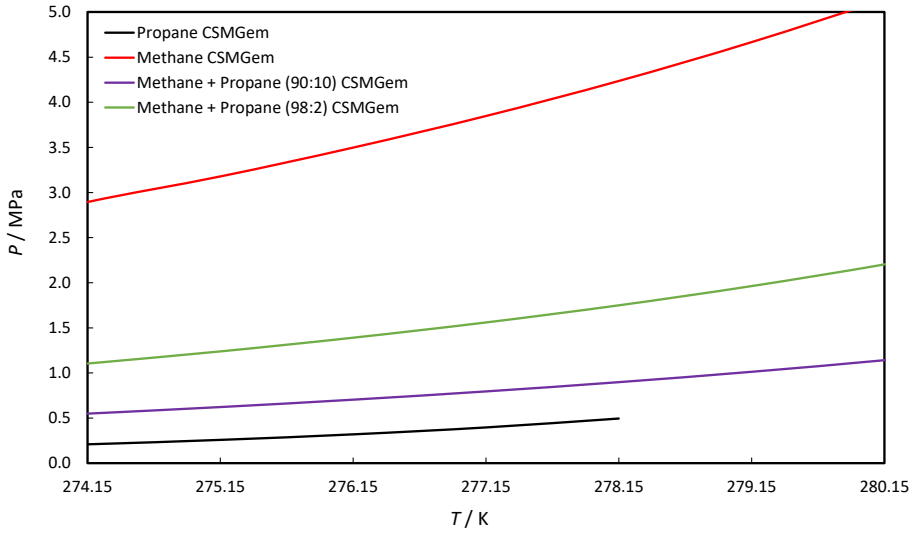

Figure 2.3: Calculated hydrate-liquid-vapor equilibrium for different guest molecules and mixtures(Sloan, 1998).

2.3 Hydrate Formation and Dissociation Kinetics

In the study of hydrate formation, not only the phase equilibria (time-independent) but also the *rates* (time-dependent) at which such compounds are formed or dissociated are to be considered. Research in gas hydrate thermodynamics has led to models that allow engineers to predict formation conditions of hydrates both in laboratory measurements and field applications (Sloan, 2004).

Among the variables that have been reported to affect the kinetics of hydrates are temperature, pressure, degree of supercooling, composition (Englezos, 1993) and the history of the water phase, also referred to as "memory effect" (Section 2.3.1.1) (Sun et al., 2010). Some kinetic processes, such as nucleation, are stochastic and seem to be dependent on instrumentation and experimental settings (Sloan, 2004; Koh et al., 2011).

The gas hydrates kinetics can be phrased in two questions: *i) how long does it take to start forming hydrates, for a given mixture and process conditions?* and *ii) what is the rate at which the hydrates will grow?* (Englezos, 1993). The answers to these questions are what is commonly referred to as *Nucleation* or *Induction Time* (subsection 2.3.1) and *Growth Rate* (subsection 2.3.2).

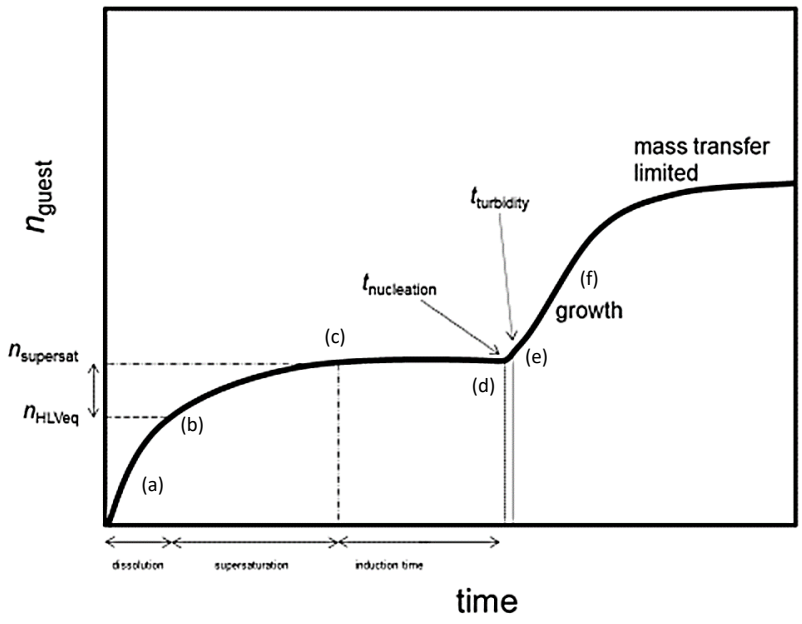

Figure 2.4: Diagram of hydrate growth at constant P and T. Moles of gas are supplied (y-axis) to a stirred batch reactor in order to maintain the pressure constant. The guest molecule dissolves in the water after pressurization (a), until reaching saturation (b) and supersaturation (c). Pressure remains constant until the first stable hydrate nuclei are formed (d). The first noticeable hydrate crystals appear (e). The hydrate phase grows readily (f). (Courtesy of J. G. Beltran. Personal communication, October 2019)

2.3.1 Nucleation and Induction Time

A diagram of a hydrate formation process is presented in Figure 2.4, in which moles of a hydrate-former gas are supplied to a stirred tank reactor to maintain a constant pressure. After pressurization, the guest gas starts to dissolve in the aqueous phase (a). Once the equilibrium concentration is reached in (b), the guest continues to dissolve until the solution reaches supersaturation (c). Supersaturation of the aqueous phase is required to form hydrate nuclei, and the higher the degree of supersaturation, the more nuclei will form in the solution (Sloan and Koh, 2008b). Nucleation occurs in the supersaturated solution when clusters of hydrates reach a maximum change in Gibb's energy (Figure 2.4-d) (Sunagawa, 2005). Any nuclei larger than these clusters in equilibrium will grow spontaneously, while any smaller nuclei will tend to dissociate. The radius of this critical cluster is often referred to as critical radius (Natarajan et al., 1994). Since nucleation occurs at a molecular level, hydrates will grow until they can be detected experimentally (Figure 2.4-e). Induction time is defined as the time elapsed between the solution achieving supersaturation and the detection of the first crystallites. As growth occurs, it is accompanied by a substantial consumption of gas molecules (Figure 2.4-f).

2.3.1.1 Memory Effect

It is a well-known experimental fact in gas hydrate systems that induction times are shorter after repeatedly forming and decomposing hydrates, compared to water with no previous history of hydrate formation (Sloan and Koh, 2008a). Hydrate formation from ice particles also yields shorter induction times.

Figure 2.5 presents an isochoric pressure and temperature trace for a series of successive hydrate formation runs. The point denoted by 'H' marks the disappearance of the last noticeable hydrate crystallite and corresponds to the hydrate-liquid-vapor equilibrium point. A pressure drop after cooling indicates hydrate growth. Although the HLV equilibrium temperature does not change with the experimental runs, the cooling required to achieve hydrate formation is reduced with each iteration (Sloan and Koh, 2008a).

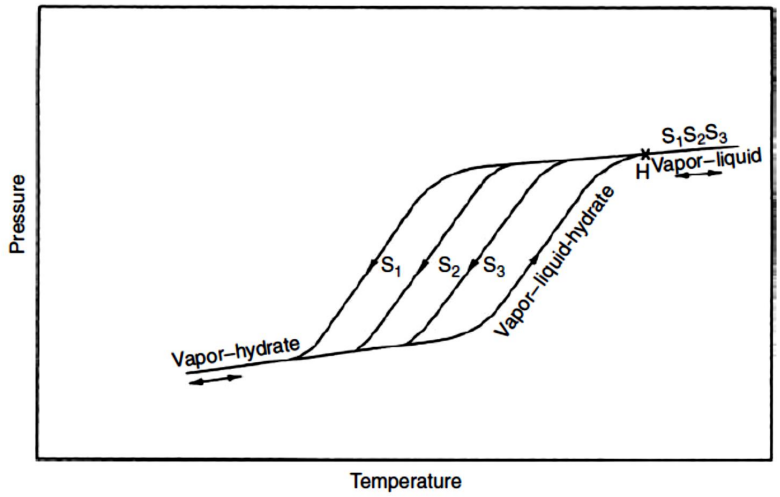

Figure 2.5: Temperature and pressure trace for cycles of hydrate formation at constant volume. S1-S3, successive cooling-heating runs. H denotes the dissociation of the last noticeable crystallite. Republished with permission of Taylor & Francis Group LLC - Books, from "Clathrate hydrates of natural gases", Sloan, E. Dendy and Koh, Carolyn A., third edition, Copyright (2008); permission conveyed through Copyright Clearance Center, Inc.

2.3.2 Growth

2.3.2.1 Mass and Heat Transfer

For growth to occur, two transport phenomena must happen simultaneously (Figure 2.6). The heat from the exothermic crystallization process must dissipate away from the growing solid phase. Solute or guest molecules move from the bulk of the liquid phase towards the growing crystals (Sunagawa, 2005; Mullin, 2001). In crystallization from solution, the solute is being concentrated significantly in the forming solid phase, compared to the diluted liquid phase; therefore mass transfer is more important in these cases (Sunagawa, 2005).

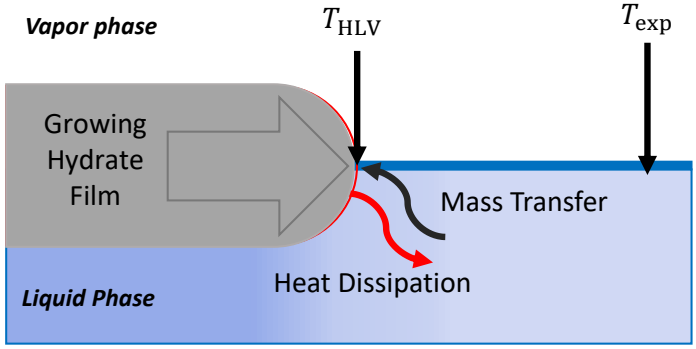

Figure 2.6: Gas hydrate film growth at the liquid-vapor interface. As the film grows, heat is dissipated away from the growing interface and guest molecules are incorporated into the growing hydrate.

If heat is being transferred efficiently, it is reasonable to assume that the hydrate-liquid-vapor interface remains at equilibrium temperature T_{HLV}, while the bulk of the liquid is at the experimental temperature. The difference between the two temperatures can be regarded as the driving force controlling this process (Equation 2.2).

$$\Delta T_{\mathrm{sub}} = T_{\mathrm{HLV}} - T_{exp} \tag{2.2}$$

2.3.2.2 Driving Force

Equilibrium is defined as a state of a system in which there is no tendency for change (Smith et al., 2001). At this state, temperature, pressure, and composition remain constant, and hydrates do not grow or dissociate. For growth to occur, the system must be taken to a state away from equilibrium into the HL region in Figure 2.7.

The driving force for crystallization formation can be generalized as the difference in chemical potentials between phases (Sunagawa, 2005). In an isobaric hydrate formation, such as the one in Figure 2.7, the experimental temperature can be set to be lower than the equilibrium temperature to form hydrates. The degree of subcooling, presented in Equation 2.2, is defined as the difference between equilibrium temperature and the experimental temperature. This magnitude is representative of the driving force in this system.

2.3.2.3 Types of Growth

After applying a driving force to the system (e.g., through subcooling) and nuclei exceeding the energy barrier for nucleation, spontaneous growth of hydrates oc-

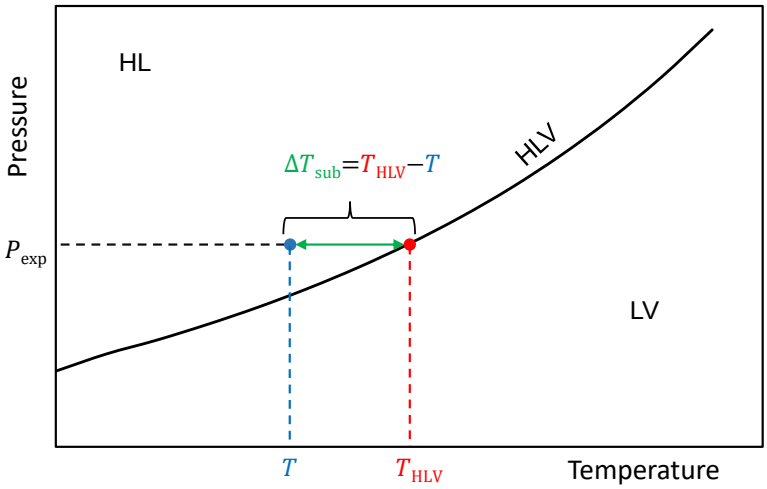

Figure 2.7: Hydrate-liquid-vapor phase diagram. P_{exp}, experimental pressure; T_{HLV}, hydrate-liquid-vapor equilibrium. ΔT_{sub}, degree of subcooling. HLV, Hydrate-liquid-vapor.

curs. The roughness of the solid interface and mechanism by which it will grow are also influenced by the driving force (Sunagawa, 2005).

As presented in Figure 2.8, as the driving force increases, the crystal surface becomes rougher. Low driving forces yield smooth surfaces that are expected to grow in spirals. As driving force increases, there is an expected transition between smooth and rough surfaces, characterized by a layer-by-layer two-dimensional growth mechanism. At higher subcoolings, the surface is rough, and the growth occurs by an adhesive-type mechanism (Sunagawa, 2005).

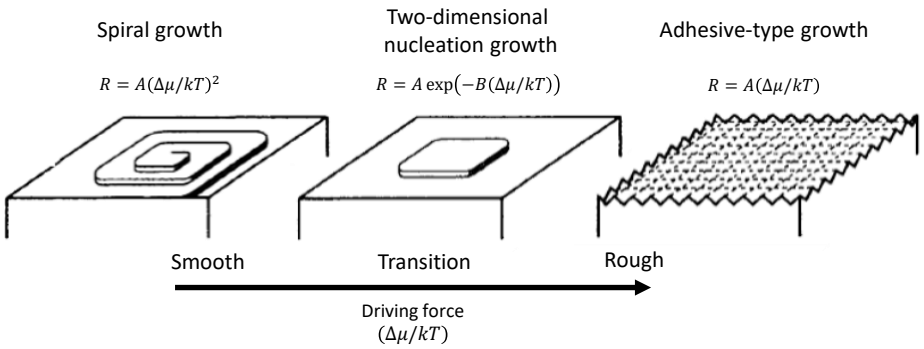

Figure 2.8: Changes in growth mechanisms and roughness of the crystal surface with increasing driving force ($\Delta\mu/kT$). Modified from Sunagawa (2005).

As presented in Figure 2.8, the expressions that relate the growth rate R to the generalized driving force $\Delta\mu/kT$ change for each growth regime (where $\Delta\mu$ is the difference in chemical potentials, k is the Boltzmann constant and T is the temperature) (Sunagawa, 2005). Growth rates increase alongside the surface roughness with the increasing driving force. Both roughness and growth rates have a strong influence on the crystal morphology (Section 2.4) (Mullin, 2001).

Due to the usual low solubilities of hydrate formers in water or that of water in the gas phase, hydrate formation will tend to occur at the water-gas interface (Sloan, 2004). In flat interfaces, single crystal growth has been reported when the driving force is small, and polycrystalline film growth is observed with larger driving forces (Li et al., 2014; Sun et al., 2010). The thickness of these films decreases with increasing subcooling (Peng et al., 2007; Lee et al., 2006).

2.3.2.4 Growth Rate

Growth rates for crystal growth increase with the increasing driving force. As mentioned before, so does the roughness of the crystal surface. In Figure 2.9, the growth rate of one crystal face as a function of driving force is presented. Critical values of the driving force ($\Delta\mu/kT^*$ and $\Delta\mu/kT^{**}$ in Figure 2.9), where the transitions between regimes are expected, have been found using computer simulations (Sunagawa, 2005).

2.4 Hydrate Crystal Morphology

A single crystal is defined as a crystal with no distortion on its faces or orientations (Sunagawa, 2005; Mullin, 2001). A solid phase comprised of several single crystals

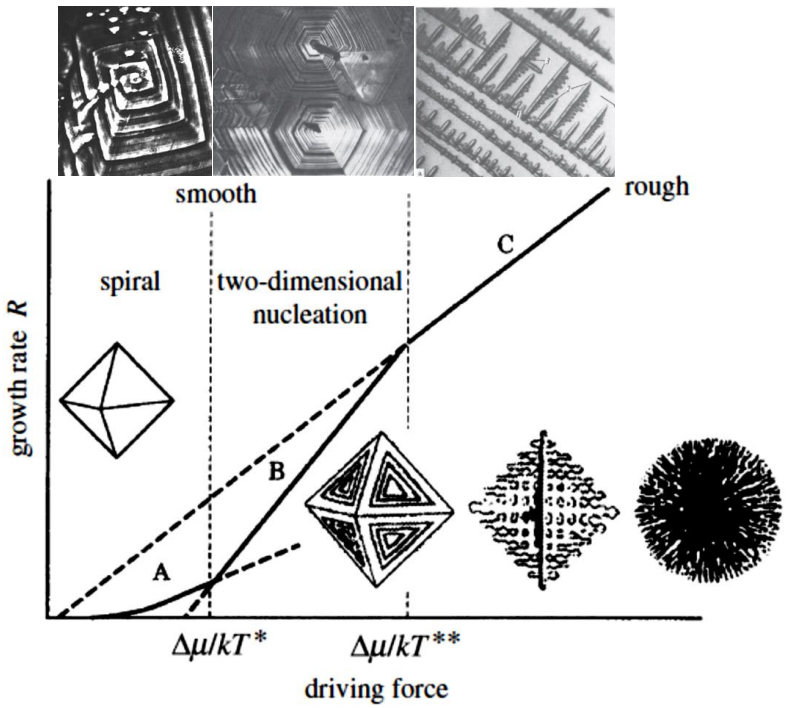

Figure 2.9: Crystal growth rate as a function of driving force. A: at lower driving forces, the crystal surface is smooth and the mechanism is spiral growth. B: transition, dominated by two-dimensional growth mechanism. C: rough crystal surface dominated by adhesive-type mechanism. Modified from Sunagawa (2005); Mullin (2001); Chernov (1984).

of different sizes and orientations is known as polycrystalline aggregate (Sunagawa, 2005).

The morphology of single crystals is determined by their crystalline structure and by the conditions leading to its growth (Sunagawa, 2005). Growth rates and mechanisms, both dependent on the driving force, can lead to different morphologies of single crystals with equal crystalline structures (Mullin, 2001). In this case, the single crystals with different morphologies are said to exhibit different "crystal habit." Solid water in snow can exhibit a hexagonal prismatic habit, or the dendritic habit in snowflakes, albeit having the same crystalline structure (Sunagawa, 2005).

2.4.1 Crystal Habit

Crystal habit is strongly determined by the relative size of the growing faces (Chernov, 1984). Due to environmental conditions, a single crystal may grow more readily in the direction of one face compared to others (Sunagawa, 2005). It is usually the slowest-growing face that determines the habit of a crystal (Chernov, 1984). Figure 2.10-a shows different crystal habits. Understanding the habits and their change with driving force could be helpful in developing more accurate models for hydrate growth.

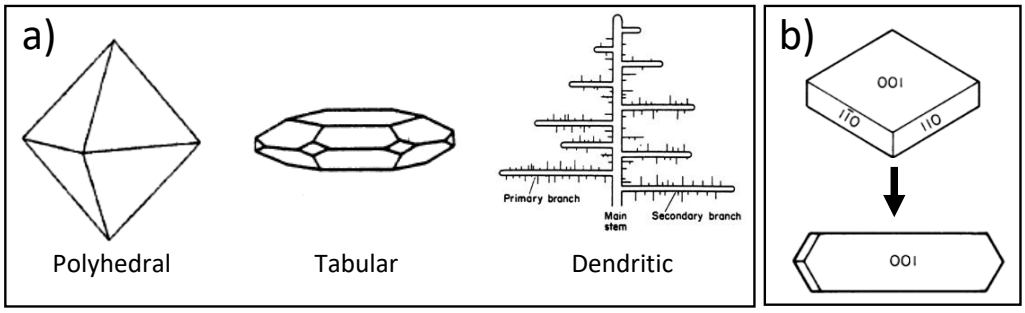

Figure 2.10: a) Some habits exhibited by crystals. b) Example of a change in habit from plate-like to an elongated blade. Modified from Sunagawa (2005); Mullin (2001).

Driving force strongly determines the crystal habit. At lower subcoolings, polyhedral, faceted, and prismatic crystals are often observed. As the driving force increases, the relative growth rates of each face change and the habit of single crystals change to flattened or elongated crystals (Mullin, 2001). At high subcoolings, rapid growth of one face compared to the others can lead to needle-like crystals. Branching stemming from these needles leads to dendritic morphologies (Mullin, 2001). An example of a change of habit from a plate-like crystal to an elongated plate or "blade" is depicted in Figure 2.10-b. It can be inferred that the (001) face grows significantly slower than the $(1\bar{1}0)$ and (110) faces, leading to a blade-like morphology.

2.4.2 Polyhedral Crystals

Polyhedral crystals (Figure 2.11) are single crystals with well-defined crystal faces. Since smooth, flat surfaces are required to grow the polyhedron faces, this crystal habit is mostly present at low driving forces (Mullin, 2001). These crystals are expected to grow by the spiral growth mechanism (Sunagawa, 2005).

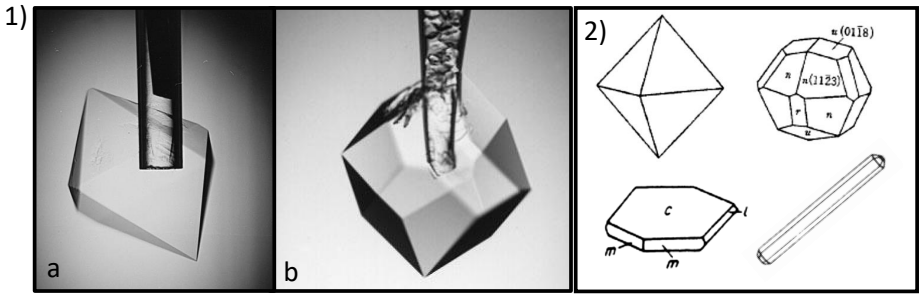

Figure 2.11: (1) Gas hydrate polyhedral crystals. (1-a), structure II tetrahydrofuran (THF) hydrate crystal (octahedron); (1-b), Structure I ethylene oxide hydrate crystal (rhombic dodecahedron). (2), Other polyhedral single crystals. Modified from Larsen et al. (1998); Mullin (2001); Sunagawa (2005).

Polyhedral crystal habit occurs when the growth rate of each face depends on its orientation and is uniform throughout the surface (Chernov, 1984). When the driving force is increased, so does the crystal growth rates and heterogeneities appear, such as local gradients of temperature and guest concentration close to the growing surface (Granasy et al., 2005). If driving force is increased, these shapes will turn into skeletal or dendritic habits (Figure 2.12) (Chernov, 1984; Ohmura et al., 2004).

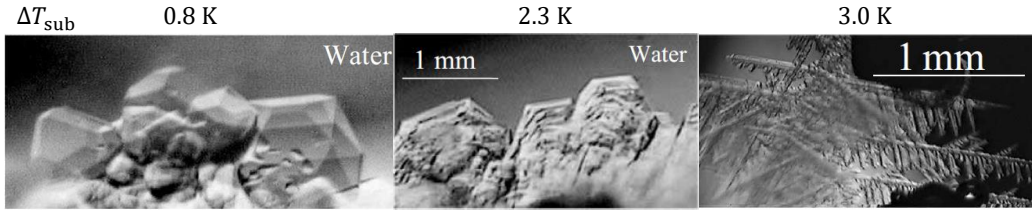

Figure 2.12: CO_2 hydrate morphology change with subcooling. Modified from Ohmura et al. (2004)

Figure 2.11-1 shows single, polyhedral hydrate crystals grown with different hydrate guests, under the same thermodynamic conditions. It can be observed that the habit of the tetrahydrofuran (THF), sII, hydrate crystal is that of an octahedron while that of ethylene oxide, sI, hydrate is a dodecahedron (Larsen et al., 1998). Hydrate polyhedral crystals have been shown to develop a dendritic habit with increasing driving force (Lee et al., 2006) and when other substances are added to the aqueous phase (Larsen et al., 1998).

Figure 2.13 presents different polyhedral crystals in gas hydrates. Methane

hydrates exhibit the same dodecahedral habit as ethylene oxide hydrate crystals in Figure 2.11 (1-b) (both sI formers) (Smelik and King, 1997; Larsen et al., 1998). The methane + propane mixture in Figure 2.13-2 exhibits the octahedral habit depicted in Figure 2.11 (1-a) (both sII) (Smelik and King, 1997; Larsen et al., 1998). This shows the influence of the crystalline structure in the development of the crystal morphology. Nonetheless, other habits can be observed for the same systems, even simultaneously (Figure 2.13-1,2). A different combination of habits can be observed in the methane + ethane system in Figure 2.13-3, in which trigonal platy crystals are formed alongside the polycrystalline film (Li et al., 2014).

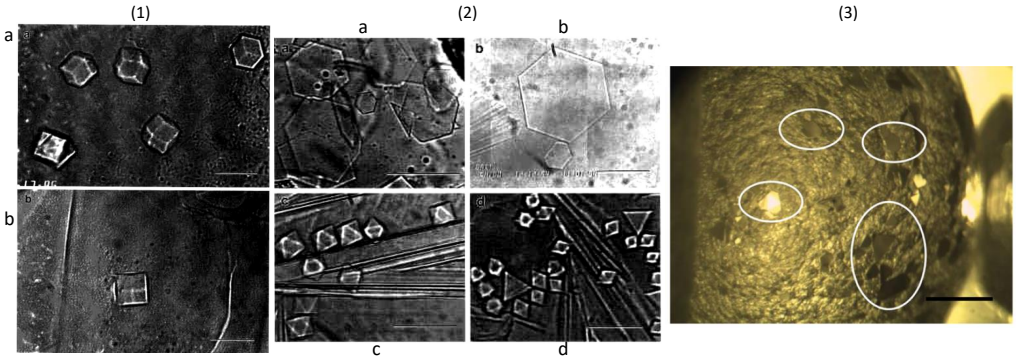

Figure 2.13: Gas hydrate single polyhedral crystals. (1) Methane hydrate crystals (sI). (1 a), rhombic dodecahedrons. (1 b), cubic habit. (2), methane + propane sII hydrate crystals (95:5 mole ratio). (2 a-b), hexagonal platelets. (2 c), octahedral crystals. (2 d), octahedrons and triangular platelets. (3) Trigonal platelets in methane + ethane sII hydrates (92.3:7.7 mole ratio). Modified from Smelik and King (1997); Li et al. (2014)

2.4.3 Single-Guest Hydrates

Several crystal habits have been reported for gas hydrates. Figure 2.14 shows crystal habit changes with respect to subcooling for methane, ethane, and propane. At low subcoolings, habit is characterized by larger crystals. However, crystals become elongated and smaller with increasing subcooling (Tanaka et al., 2009).

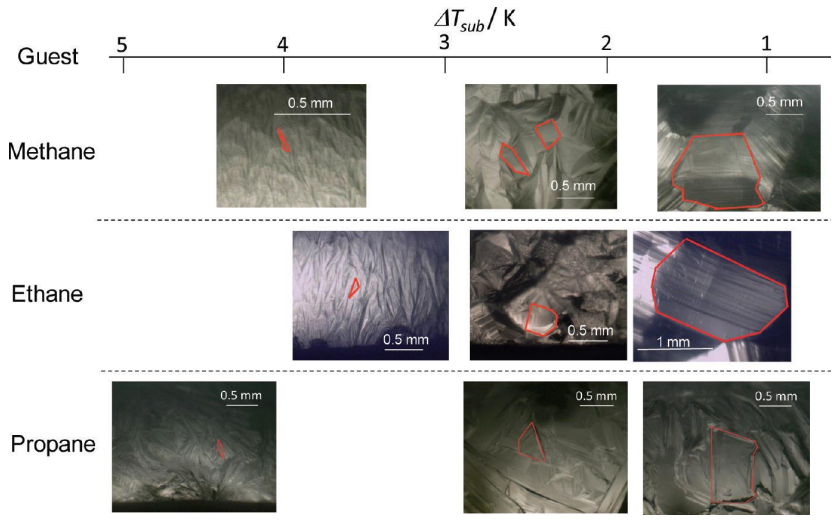

Figure 2.14: Changes in hydrate crystal habit with respect to subcooling and guest. Reprinted with permission from R. Tanaka, R. Sakemoto, R. Ohmura, Crystal Growth and Design, 2009, 9, 2529. Copyright (2009) American Chemical Society.

At higher subcoolings the differences in habit become less evident. Some studies have observed a change from polyhedral to granular morphologies with increasing subcooling (DuQuensay et al., 2016; Li et al., 2014). Other authors observed a transition from granular to dendritic crystal habit with increasing subcooling (Li et al., 2014; Ohmura et al., 2004; Freer et al., 2001; Ohmura et al., 2005b; Ueno et al., 2015).

2.4.4 Mixed Hydrates

Mixed hydrates exhibit a wide range of morphologies that change with the composition of the vapor phase. Figure 2.15-1 shows methane + ethane hydrate habit change with respect to subcooling and methane content in the vapor phase. In this system, a faceted crystal film is observed to grow when ethane is present. Morphology seems to be dominated by the presence of ethane (Li et al., 2014). A similar trend was observed by Saito et al. (2011) in hydrates formed from methane + ethane + propane ternary mixtures(Figure 2.15-2). Regardless of the initial gas mixture composition, differences in crystal habit become less evident with increasing subcooling.

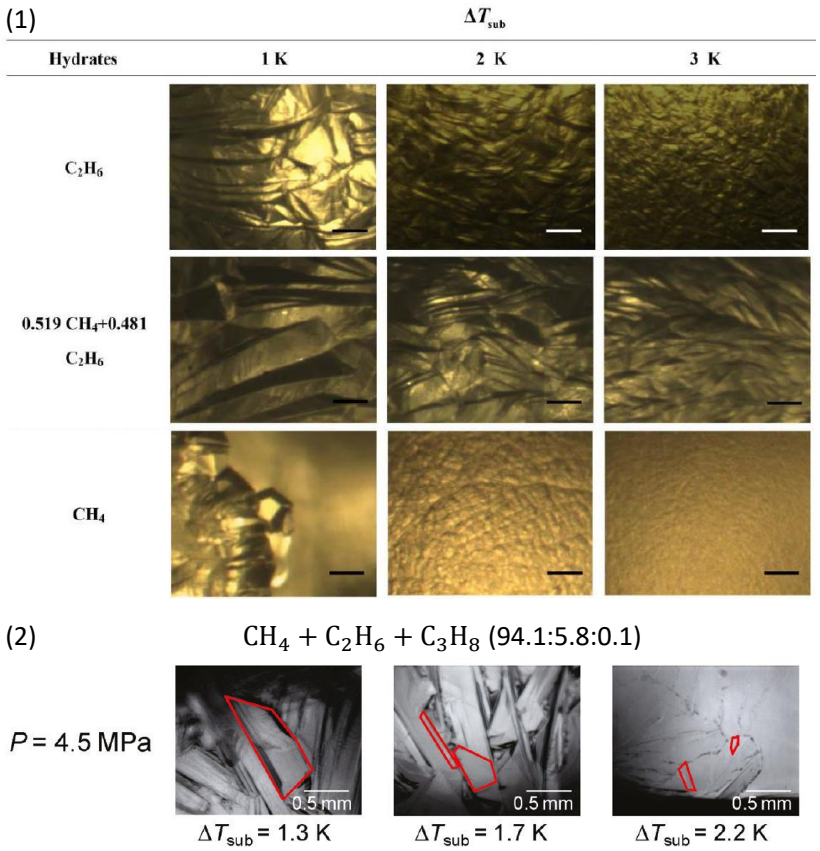

Figure 2.15: Changes in mixed gas hydrate crystal habit with respect to subcooling.(1), hydrates formed with methane + propane binary gas mixtures of different compositions; (2), Hydrates formed with a methane + ethane + propane ternary mixture. Modified from Li et al. (2014) and Saito et al. (2011)

Polyhedral crystals have been observed to grow alongside the polycrystalline hydrate film (Li et al., 2014; DuQuensay et al., 2016). It has been hypothesized that these individual crystals can have a different crystalline structure than the film (Li et al., 2014). In methane + propane and methane + ethane hydrates, different crystalline structures can coexist in the hydrate phase and exhibit different morphologies (Schicks et al., 2006; Li et al., 2014).

2.4.4.1 Transformations in Methane + Propane Hydrates

A pseudo-P-x diagram of the methane + propane is presented in Figure 2.16. It can be seen that in methane mole fractions greater than 0.94, sI and sII phases can coexist (Ballard and Sloan, 2001). The presence of these different structures

is an example of polymorphism (Mullin, 2001). Polymorphs can transform into their most stable forms with changes in thermodynamic conditions (Mullin, 2001).

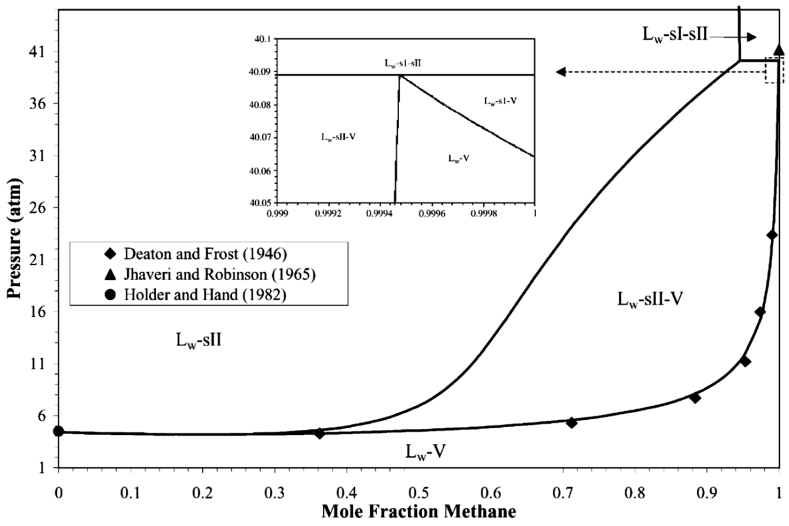

Figure 2.16: Pseudo P-x diagram for methane-propane-water system at 277.6 K. The region at the upper-right corner in the diagram represents the $P - x$ conditions at which structures I and II coexist. Reprinted from Chemical Engineering Science, 56/24, A.L. Ballard and E.D. Sloan, Hydrate phase diagrams for methane + ethane + propane mixtures, 6883-6889, Copyright (2001), with permission from Elsevier.

Polymorph transformations in gas hydrates have been observed as some crystals dissociated and recrystallized into their most stable forms (Schicks and Ripmeester, 2004; Schicks et al., 2006). In this sense, transformations can lead to a change of morphology, but a change in habit does not necessarily constitute a transformation. Each polymorph constitutes a phase, whereas crystals with the same structure and exhibiting different habits, constitute a single phase (Mullin, 2001).

One of such transformations for the methane + propane system is presented in Figure 2.17 (blue markers and curve). This system, studied by Schicks et al. (2006), has two regions with different crystalline structures present. In area 1, only sI hydrates are observed to form. Figure 2.17-a shows the hydrate morphology in this area. After cooling the system, a sudden change in morphology occurs, as shown in Figure 2.17-b. After characterizing the hydrates using Raman spectroscopy, Schicks et al. (2006) found that in area 2 structures I and II coexist. This process appears to be reversible, with the transition temperature

being close to the T_{HLV} of methane hydrates at the same pressure (Figure 2.17-c, dashed curve) (Schicks et al., 2006).

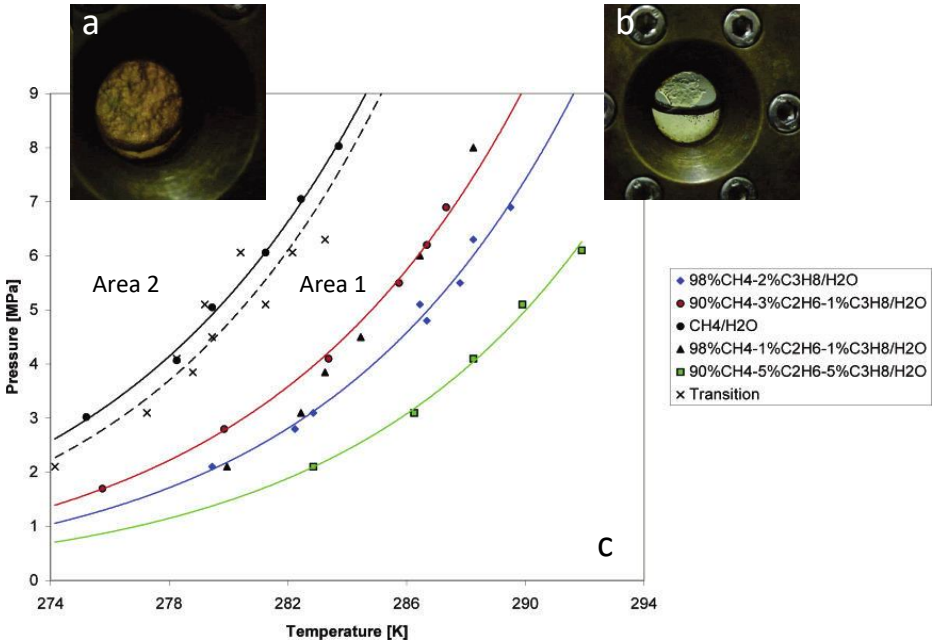

Figure 2.17: Transformations in mixed gas hydrates. a) Hydrate morphology before the transformation. (b), hydrate morphology after the transformation; (c), phase diagram showing decomposition curves for different systems (solid) and transition curve (dashed); The methane + propane ($y_{\mathrm{CH_4}} = 0.98$ gas mixture) system is presented in blue. Area 1: sI hydrates; area 2: sI + sII hydrates. Modified from Schicks et al. (2006).

2.5 Experimental Methods and Apparatuses

In this section, equipment and methodologies used for the study of crystalline structures, phase equilibria, kinetics, and morphology of gas hydrates are presented. A description of the 3-in-1 method is presented as well.

2.5.1 Structure of hydrates

Spectroscopic methods are used to identify crystalline structures, rates at which a guest is included in the hydrate cages (i.e., enclathration rates), and cage occupancies. Nuclear magnetic resonance has been used to identify the hydrate crystalline structure formed by hydrates. Ripmeester et al. (1987) identified in

1987 the hexagonal structure H using a combination of nuclear magnetic resonance (NMR), and x-ray and neutron powder diffraction. Enclathration rates in mixed hydrates have been measured using ^{13}C NMR (Fleyfel et al., 1993; Kini et al., 2004).

Raman spectroscopy also has been used for structural identification. Uchida et al. (2004) identified structures I and II on methane + propane hydrates in a two-step formation process using Raman spectroscopy and x-ray diffraction. Schicks et al. (2006) observed hydrates formed from hydrocarbon mixtures transforming from sI to a mixed-phase comprised of sI and sII using x-ray diffraction and Raman spectroscopy. Schicks and Ripmeester (2004) demonstrated the coexistence of sI and sII methane hydrate using Raman spectroscopy. Cage occupancy and enclathration rates were also identified by Schicks and Luzi-Helbing (2013) using time-depending Raman spectroscopy measurements.

2.5.2 Phase equilibria

Pressure and temperature are the most commonly controlled and measured variables in hydrate investigations. Measurements of phase equilibria are often presented in terms of these variables (Sloan and Koh, 2008a). Identifying PT equilibrium points on single hydrates require controlling one of the variables and measuring the other (Section 2.1).

By maintaining a constant temperature in a pressurized vessel, the HLV equilibrium pressure can be measured. One such method is known as the "pressure search method" (Englezos and Ngan, 1994). The pressure-search method consists of rapid hydrate formation by increasing the pressure at a constant temperature, followed by dissociation achieved by reducing the pressure. The final step consists of increasing the pressure in small steps. The hydrate formation point is determined when trace amounts of hydrates appear in the vessel, with no changes in pressure or temperature (Mei et al., 1996; Wu and Englezos, 2006). It has been reported that at least 6 to 12 hours are required to obtain a single equilibrium datum with this method (Beltran and Servio, 2008).

By maintaining a constant volume, the equilibrium point can be measured from the pressure response to a cycle of heating and cooling in a pressurized vessel, known as the isochoric (PVT) method. This method consists of cycles of cooling and heating (0.2 - 0.05 K/h), in which pressure changes are recorded on a PT trace. Rapid pressure drop upon cooling indicates hydrate formation, while a sudden increase of pressure upon heating indicates hydrate dissociation. The hydrate-liquid-vapor equilibrium point is given by the intersection of the cooling and heating PT curves (de Menezes et al., 2019; Hu et al., 2017; Chu et al., 2016). In an analogous way to the pressure search method, the equilibrium point can be determined at constant pressure by measuring the temperature at which the last noticeable hydrate crystals dissociate. These isobaric methods take several hours

per datum, due in part to the slow heating rates used to avoid overestimating the equilibrium temperature (Tohidi et al., 2000).

High-pressure differential scanning calorimetry has also been used to measure the T_{HLV} at constant pressure. The technique also allows measuring other properties such as enthalpy of formation and heat capacity (Zhang et al., 2004). By plotting the heat flow to the sample against temperature, the formation and dissociation are identified as peaks in this thermogram. The onset of the dissociation peak is used to estimate the equilibrium temperature of the hydrate sample (de Menezes et al., 2019; Davies et al., 2009; Zhang et al., 2004).

2.5.3 Kinetics

Gas uptake methodologies are often used to evaluate the kinetics of formation in gas hydrates (Section 2.3.1). The method consists of feeding gas to maintain constant pressure to a tank reactor at a constant temperature (Vysniauskas and Bishnoi, 1983). Induction times can be measured as the time elapsed between supersaturation and the start of hydrate growth, marked by rapid gas consumption (Englezos et al., 1987).

Some of the methods used for structural analysis, such as neutron diffraction, x-ray diffraction, NMR, and Raman spectroscopy, have also been used to evaluate the kinetics of hydrate formation. By tracking the formation of the hydrate phases over time, the rate at which the single or multiple guests enclathrate can be measured (Schicks and Luzi-Helbing, 2013; Kini et al., 2004; Klapproth et al., 2019).

Some kinetic studies measure lateral growth rates of polycrystalline films at the liquid-vapor interface. These techniques have allowed identifying the growth rates dependency on subcooling, and differences in growth kinetics depending on guests and additives in the system (Freer et al., 2001; Tanaka et al., 2009; Peng et al., 2007; Saito et al., 2011; Li et al., 2014).

2.5.4 Morphology

Optical cells are widely used to evaluate hydrate morphology and film growth rates. Cells usually consist of a pressurized vessel containing a liquid sample ranging from 10 to 250 mL, with sight windows. Some morphology studies are conducted on water droplets inside the pressure cells (Lee et al., 2005; Ohmura et al., 2005a; Servio and Englezos, 2003), and using different substrates to hold the droplets (Esmail and Beltran, 2016). Larger liquid samples have been used to evaluate hydrate formation within the aqueous phase (Ohmura et al., 2004, 2005b; Lee et al., 2005). Hydrate formation on gas bubbles suspended in the aqueous phase also has been performed (Lee et al., 2014; Li et al., 2014; Peng et al., 2007). These techniques provide information on the morphology of hydrate films at the

liquid-gas interface, single crystals, growth mechanisms, and their dependence on subcooling, the composition of the vapor phase, and the presence of additives.

2.5.5 Beltran's 3-in-1 approach

DuQuensay et al. (2016) designed a high-pressure, bilateral temperature control stage to study hydrate formation with tight control of the crystallization substrate temperature. The temperature-control stage is placed inside a high-pressure vessel with axial sight windows. A sapphire slide is used to hold the water samples. The stage allows uniform temperature or constant temperature gradient profiles across the sapphire substrate.

This apparatus can provide valuable information on morphology, apparent kinetics, and phase equilibria, with a single experimental setup (DuQuensay et al., 2016). The technique has also been used to study methane hydrates in the presence of classic inhibitors (Kumar, 2016) as well as commercial hydrate inhibitors (Ovalle et al., 2019). Differences between methane and carbon dioxide gas hydrates have been studied using this technique (Sandoval, 2015) as well as mixtures of these two guests (Ortiz, 2017).

The 3-in-1 technique has shown minimum experimental uncertainties and high precision in phase equilibria and hydrate-film growth rate measurements (Sandoval, 2015; Ortiz, 2017; Ovalle et al., 2019). High-resolution imaging of the hydrate morphology has been obtained for the aforementioned systems.

2.5.5.1 Phase Equilibria

Both thermoelectric coolers on the stage can be set at different temperatures to a constant gradient across the slide. If the temperatures of both TEC modules are increased in steps, while keeping the temperature gradient constant, the dissociation of the hydrates can also be controlled in steps (Figure 2.18).

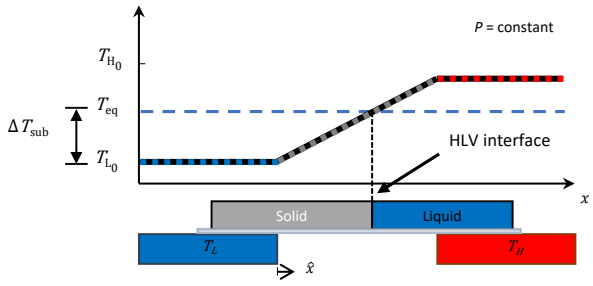

Figure 2.18: A constant temperature gradient is applied to the substrate. By increasing the temperature of both ends and keeping the gradient across the slide constant, the hydrate-liquid-vapor interface can be moved in steps. Adapted from (DuQuesnay, 2014).

Since at each dissociation step the temperature of the solid-liquid interface must be the equilibrium temperature (T_{HLV}), each step becomes a replicate of hydrate-liquid-vapor equilibrium conditions of the system (Figure 2.19).

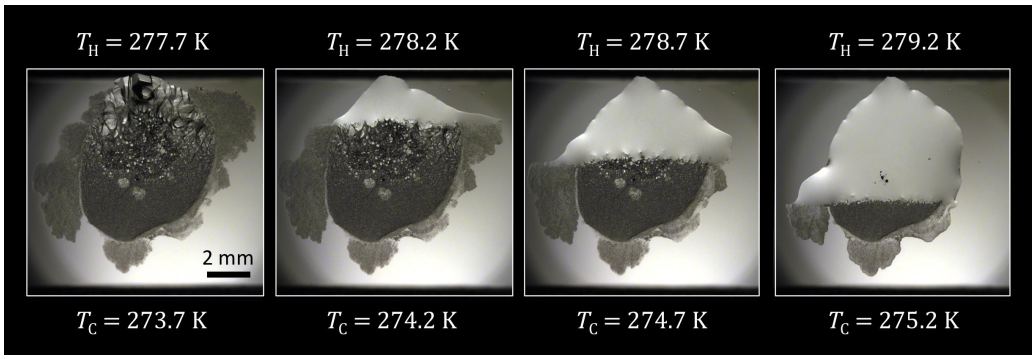

Figure 2.19: Dissociation sequence of methane hydrates using a temperature gradient. The liquid-hydrate interface is at T_{HLV}. Reproduced from (DuQuesnay, 2014).

2.5.5.2 Kinetics

To measure apparent growth kinetics, the technique allows tracking the position of the hydrate film over time. Thus, it is possible to calculate the velocity at which hydrates grow and the dependence on subcooling, among other variables.

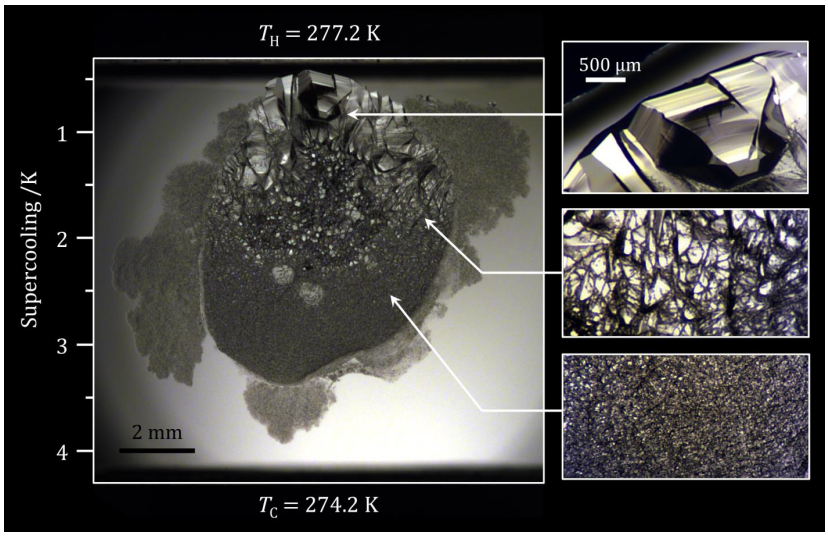

Figure 2.20: Methane hydrate formed under a constant temperature gradient. Reproduced from (DuQuesnay, 2014).

2.5.5.3 Morphology and Growth

A temperature gradient can be used to grow hydrates under several degrees of subcooling in a single experiment. Figure 2.20 shows the morphology of methane hydrates formed under a constant temperature gradient. The technique allows to quickly identify the morphology dependence on subcooling and to obtain magnified images of the crystal morphology. Uniform temperature formation can also be used to evaluate the morphology at the desired subcooling.

Chapter 3

Experimental

3.1 Apparatus

This work uses a modified version of the apparatus designed by DuQuensay et al. (2016). The apparatus consists of a high-pressure vessel containing a bilateral temperature control stage.

A schematic of the apparatus is presented in Figure 3.1. It consists of a 316 stainless steel, high-pressure vessel, with high-pressure sapphire sight windows located axially in the vessel for visual inspection (Rayotek, CA, USA) (Figure 3.1-B). The reactor temperature was controlled using an AC200 refrigerated circulator (Fisher Scientific, Canada) (Figure 3.1- F). Aqueous ethylene glycol (50% by volume) was used as the cooling fluid, flowing through a copper coil jacket, wrapped around the body of the vessel (Figure 3.1-E). The temperature inside the vessel was measured using a platinum RTD probe with a standard instrumental uncertainty of $u_{T_{\mathrm{RTD}}} = 0.32$ K (Omega Engineering, QC, Canada). Pressure was measured using a Rosemont 3051s pressure transmitter with a standard instrumental uncertainty of $u_{P_{\mathrm{Transm.}}} = 0.005$ MPa (Laurentide Controls, QC, Canada). A Schott KL2500 LCD cold light source (Optikon, ON, Canada) was used for illumination of the vessel (Figure 3.1-D).

3.1.1 Temperature control stage

Crystallization temperature was controlled using a high-pressure bilateral temperature control stage, modified from the original design by DuQuensay et al. (2016) (Figure 3.2). The stage is comprised of two independently-controlled thermoelectric cooler modules (TECs), placed on both ends of the stage (TE Technology, MI, USA) (Figure 3.2-A). To ensure an even temperature distribution, two copper plates were attached to the top and bottom of each TEC (Figure 3.2-B). The temperature of each plate was measured using fast-response thermistors with a standard instrumental uncertainty of $u_{T_{\mathrm{Thermistor}}} = 0.01$ K. A sapphire slide was

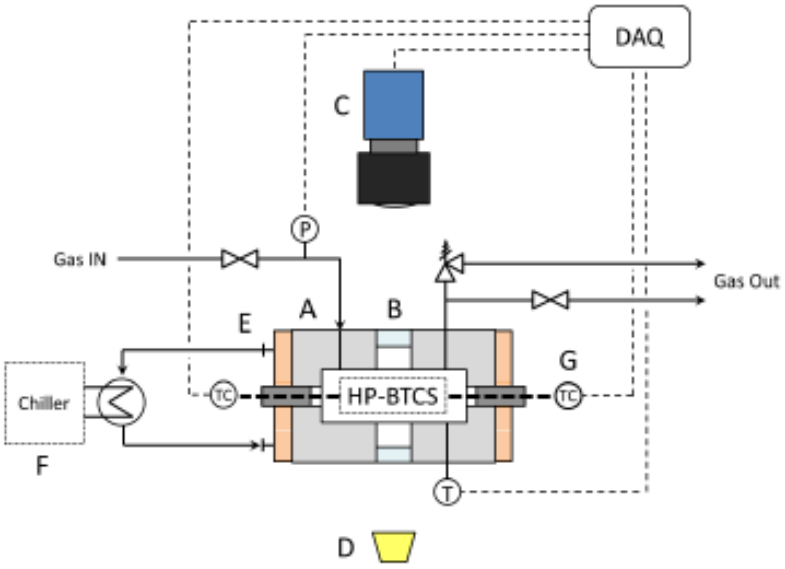

Figure 3.1: Diagram of the hydrate reactor designed by DuQuensay et al. (2016).(A) 316 stainless steel pressure vessel. (B) Sapphire sight windows. (C) Video camera. (D) Cold light source. (E) Coolant jacket. (F) Refrigerated circulator. (G) Bi-polar PID temperature controllers. Modified from (Duquesnay et al., 2016)

placed on top of the copper plates to hold the liquid sample (Meller Optics, RI, USA) (Figure 3.2-C). Temperature was controlled using bi-polar PID temperature controllers, with a resolution of ±0.01 K (TE Technology, MI, USA).

3.1.2 Imaging

High-resolution imaging was obtained using a PCO.edge 5.5 sCMOS camera (Optikon, ON, Canada) (Figure 3.1-C), fitted to either a NIKON AF-Micro-Nikkor 60 mm lens (Optikon, ON, Canada), or an Infinity KC long-distance Microscope (Optikon, ON, Canada).

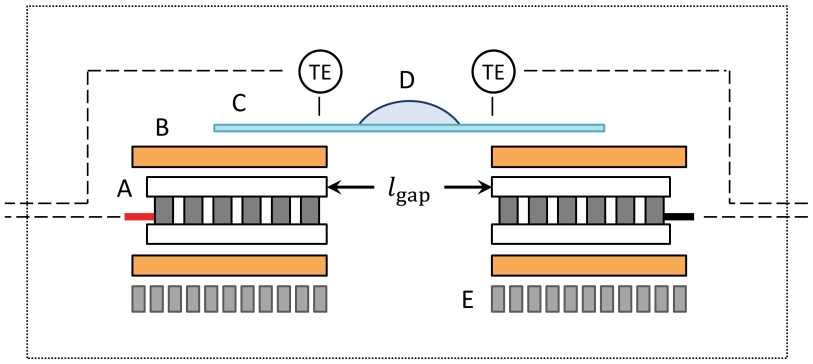

Figure 3.2: High-pressure bilateral temperature control stage. (A), Thermoelectric cooling modules (TECs); (B), copper plates; (C), sapphire microscope slide; (D), liquid sample; (E), heat sink. Modified from (Duquesnay et al., 2016).

3.2 Materials and Methods

Before each experiment, the sapphire slide was cleaned with liquid detergent and rinsed thoroughly with deionized water. The slide was submerged in acetone for five minutes and then submerged in isopropanol for five minutes in a sonication bath. The slide was dried using compressed air and placed on top of the copper plates on the stage. A 20 μL droplet of deionized water was placed on the sapphire slide using a micropipette. The vessel was sealed and was purged three times with nitrogen (Table 3.1). The vessel was purged three times with the appropriate methane + propane gas mixture, presented in Table 3.2. The mixtures were selected to allow the formation of hydrates with different crystalline structures (Ballard and Sloan, 2001).

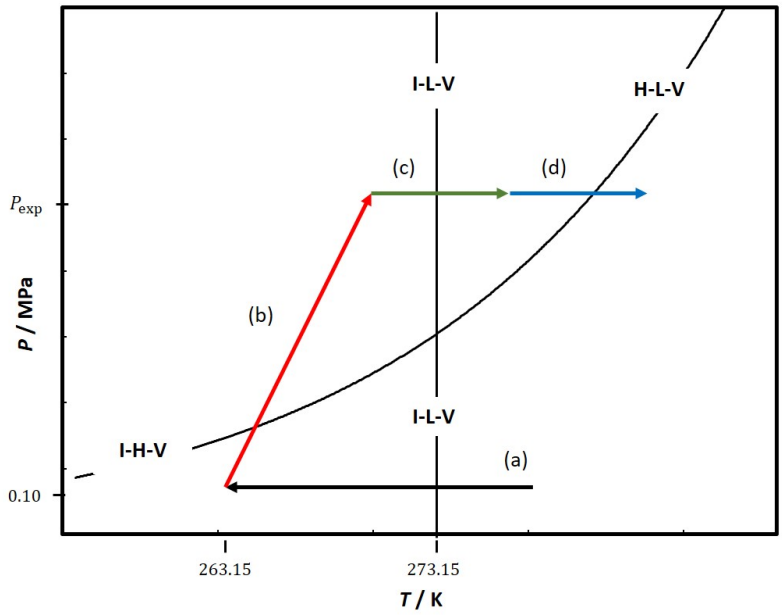

Figure 3.3: Pretreatment of the water droplets. (a), Droplet is cooled at a constant pressure slightly above 0.1 MPa; (b), after ice formation, pressure is increased to the experimental pressure to form hydrates; (c), temperature is increased to melt the ice and leave only hydrates; (d), temperature is increased to dissociate hydrates. Modified from (Kumar, 2016).

Table 3.1: Other reagents used in this study. Resistivity was used as an indicator of water purity: at the source, it was measured to be 18 MΩ·cm

Chemical name	Source	Purity	Purity units
N_2	Air Liquide, QC, Canada	99.99	mole fraction
Distilled water	In-house	See caption	See caption

Table 3.2: Gas mixtures used in this study

	Nominal mole fraction		Actual mole fraction		
	$10^2\ y_{CH_4}$	$10^2\ y_{C_3H_8}$	$10^2\ y_{CH_4}$	$10^2\ y_{C_3H_8}$	Source
Mixture 1	90	10	90.001	9.999	Air Liquide, QC, Canada
Mixture 2	98	2	97.999	2.001	

3.2.1 Pretreatment

Pretreatment of the sample is presented in Figure 3.3. The sample was cooled at a constant pressure slightly above 0.1 MPa to form ice (Figure 3.3-a). After ice was formed, the vessel was pressurized to the experimental pressure (Figure 3.3-b). The temperature was increased to melt the ice, leaving only hydrates (Figure 3.3-c). The hydrates were dissociated by increasing the temperature above the hydrate-liquid-vapor equilibrium curve (Figure 3.3-d). After the last noticeable hydrate crystallite dissociated, a hydrate formation experiment was performed.

3.2.2 Hydrate formation

The liquid sample was crystallized using a constant temperature gradient and a uniform temperature profile. In the constant temperature gradient, the two TECs were set at temperatures below the hydrate-vapor-liquid equilibrium temperature, with a temperature difference of 5 K across the stage, resulting in a temperature gradient of approximately 0.45 K·mm^{-1} (Figure 3.4-a). This allows hydrates to form at several different subcoolings across the water droplet in a single experiment. For uniform temperature formation, both TECs were set at the same temperature below the equilibrium temperature, providing a single subcooling for crystallization of the entire droplet (Figure 3.4-b). Table 3.3 presents the experimental conditions used in uniform temperature profile experiments ($T_h = T_c$), and constant temperature gradient profile experiments ($T_h - T_c = 5$ K; gradient is approximately 0.45 K·mm^{-1}).

3.2.3 Hydrate dissociation

Controlled hydrate dissociation was achieved by establishing a constant temperature gradient across the slide (Figure 3.5). Temperature of both ends of the stage was increased simultaneously, in steps of 0.5 K. After dissociation in the droplet was observed, the steps were set to 0.2 K, and increased every 30 min. Since the temperature gradient across the sapphire slide was found to be linear by DuQuensay et al. (2016), the temperature at the interface can be measured at each step. Since hydrate-liquid-vapor phases coexist at the interface at each step, this temperature corresponds to the T_{HLV} at the experimental pressure. The average of the temperatures at the interface at each step is reported.

3.2.4 Experiments

All experiments were performed at constant pressure conditions. After pretreatment of the droplet, hydrate formation was achieved using uniform surface temperature or a constant temperature gradient profiles. Table 3.4 summarizes the experimental data per water droplet and per formation cycle.

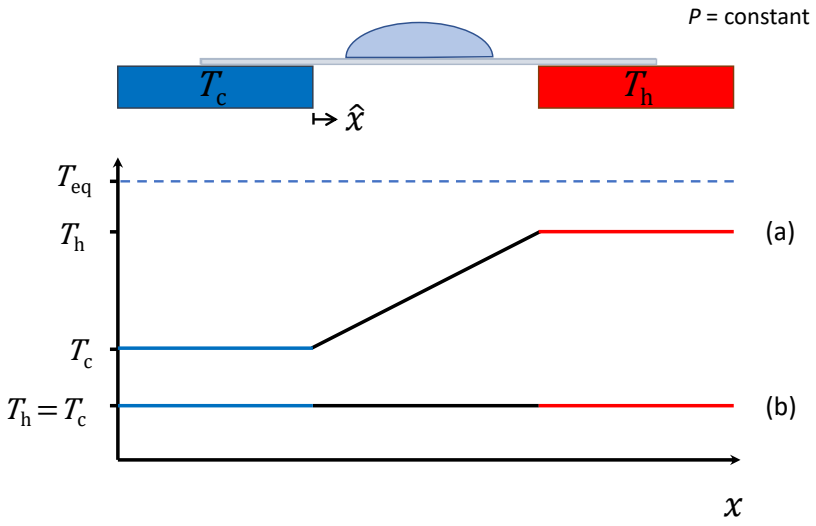

Figure 3.4: Hydrate formation profiles. T_{h}, hot plate; T_{c}, cold plate; (T_{eq}), hydrate-liquid-vapor equilibrium temperature (T_{HLV}); (a), constant temperature gradient profile; (b), uniform temperature profile.

Table 3.3: Methane + propane hydrate formation conditions in this work. P, experimental pressure; T_{HLV}, hydrate-liquid-vapor equilibrium temperature; T_{h}, temperature of the hot plate; T_{c}, temperature of the cold plate; ΔT_{sub}, subcooling.

CH_4:C_3H_8 (nominal mole ratio)	P/MPa	T_{HLV}/K	T_{h}/K	T_{c}/K	ΔT_{sub}/K
90:10	1.6	283.0	282.5	282.5	0.5
			282.0	282.0	1.0
			281.5	281.5	1.5
			281.0	281.0	2.0
			280.5	280.5	2.5
			280.0	280.0	3.0
			279.5	279.5	3.5
			279.0	279.0	4.0
			278.5	278.5	4.5
			278.0	278.0	5.0
	0.8	277.4	277.7	271.7	1.0-4.7
98:2	1.5	277.3	276.2	276.2	1.1
			275.2	275.2	2.0
	2.1	280.5	277.5	277.5	3.0
			276.5	276.5	4.0
			275.4	275.4	5.1
	1.5	277.3	278.2	273.2	0.5-4.1

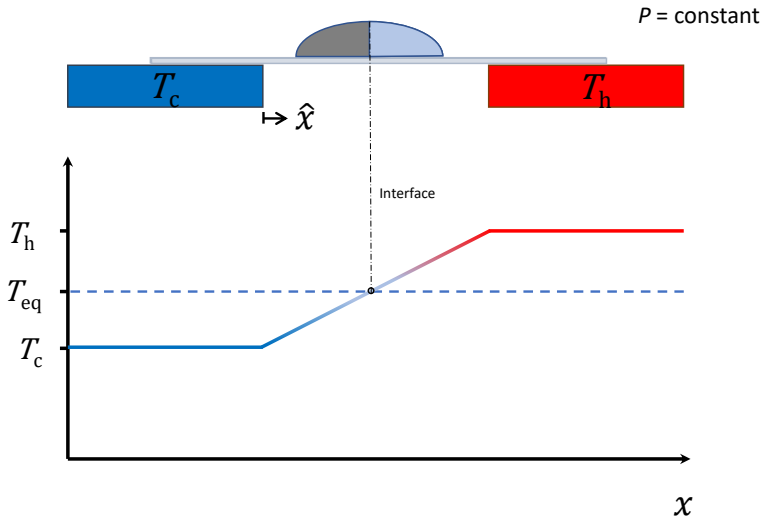

Figure 3.5: Controlled hydrate dissociation. T_h, hot plate; T_c, cold plate; T_{eq}, hydrate-liquid-vapor equilibrium temperature (T_{HLV}).

Table 3.4: Summary of pressures, equilibrium temperatures, number of experimental set-ups and experimental runs in this work. P, experimental pressure; T_{HLV}, hydrate-liquid-vapor equilibrium temperature; *, nominal molar concentration.

Nominal concentration				Formation cycles		
$10^2\ y_{CH_4}$	P/MPa	T_{HLV}/K	Droplets	Uniform T.	Const. T. Grad.	Grad. Diss.
90	0.7	276.6	3	3	6	3
	0.8	277.4	5	20	6	3
	0.9	278.3	3	3	0	3
	1.0	279.4	3	14	2	3
	1.1	279.8	3	3	0	3
	1.3	281.4	3	3	0	3
	1.6	283.0	27	137	3	3
98	1.5	277.3	3	5	2	4
	2.1	280.3	9	12	0	4
	Total		**59**	**200**	**19**	**29**

Chapter 4

Results

4.1 Morphology and Growth Mechanisms

4.1.1 The methane + propane ($y_{\mathrm{CH_4}} = 0.90$ mixture) system

4.1.1.1 Uniform Surface Temperature

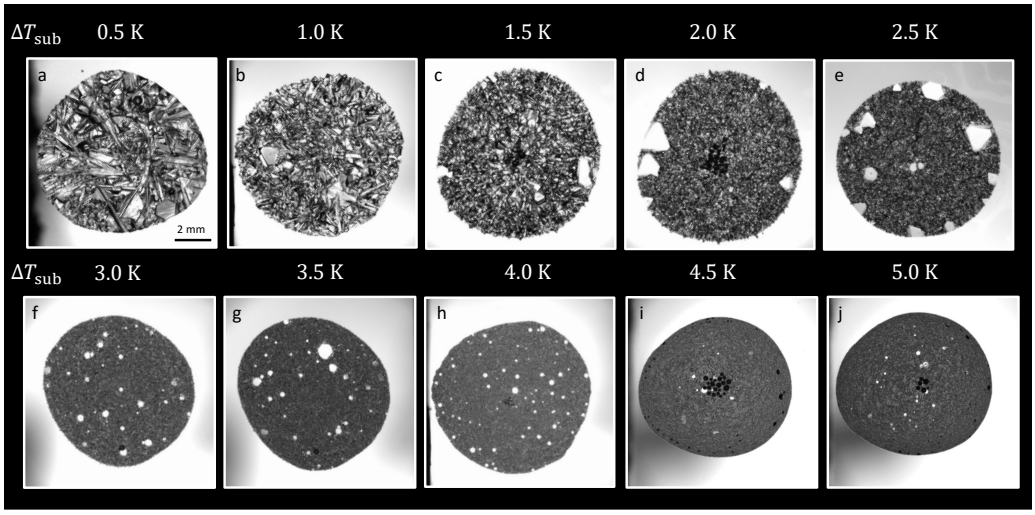

Figure 4.1: Methane + propane ($y_{\mathrm{CH_4}} = 0.90$ gas mixture) hydrates formed under uniform surface temperature. (a-j): $P = 1.6$ MPa, $T_{\mathrm{HLV}} = 283.02$ K. (a), $T = 282.5$ K. (b), $T = 282.0$ K. (c), $T = 281.5$ K. (d), $T = 281.0$ K. (e), $T = 280.5$ K. (f), $T = 280.0$ K. (g), $T = 279.5$ K. (h), $T = 279.0$ K. (i), $T = 278.5$ K. (j), $T = 278.0$ K.

Figure 4.1 presents methane + propane ($y_{CH_4} = 0.90$ gas mixture) hydrates formed under uniform surface temperature at constant pressure. The crystal habit became smoother as individual crystals became smaller with increasing subcooling. Three groups of crystal habits were identified based on the morphology of the film and single crystals: A coarser hydrate film at $\Delta T_{sub} \leq 1.5$ K (Figure 4.1, (a-c)); an intermediate group at $2.0 \leq \Delta T_{sub} \leq 3.5$ K (Figure 4.1, (d-f)) and a darker, smoother crystal habit at $\Delta T_{sub} \geq 4.0$ K (Figure 4.1, (g-j)).

Big polyhedral crystals were observed embedded in the crystal film. Although these crystals were observed throughout all the studied subcoolings, they were mostly present at a range of subcoolings between 2.0 K and 4.0 K (Figure 4.1, (d-h)). The morphologies of individual crystals included hexagonal, trigonal and triangular platelets, blades, and needles. The most common morphology of single crystals was the trigonal platelet, which can be seen in Figure 4.1 at $1.5 \leq \Delta T_{sub} \leq 3.5$ K. As subcooling increased, hexagonal morphologies became dominant (Figure 4.2).

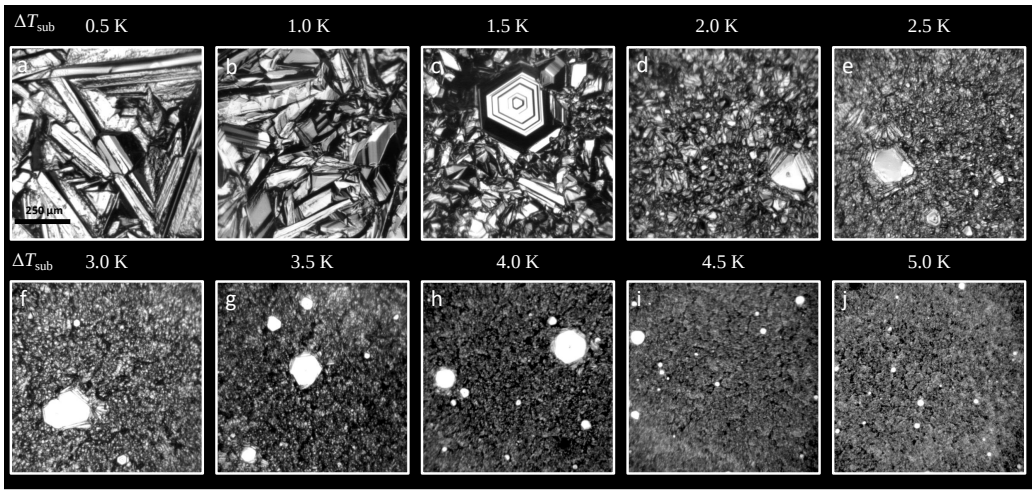

Figure 4.2: Magnified images of methane + propane ($y_{CH_4} = 0.90$ gas mixture) hydrates, formed under uniform surface temperature. (a-j): $P = 1.6$ MPa. $T_{HLV} = 283.02$ K. (a), $T = 282.5$ K. (b), $T = 282.0$ K. (c), $T = 281.5$ K. (d), $T = 281.0$ K. (e), $T = 280.5$ K. (f), $T = 280.0$ K. (g), $T = 279.5$ K. (h), $T = 279.0$ K. (i), $T = 278.5$ K. (j), $T = 278.0$ K.

Figure 4.2 shows magnified images of the crystal habit of hydrates formed with the $y_{CH_4} = 0.90$ gas mixture at several subcoolings. Based on the film morphology, crystal habits were separated into three groups: between $0.5 \leq \Delta T_{sub} \leq 1.5$ K (Figure 4.2, (a-c)); between 2.0 K $\leq \Delta T_{sub} \leq 3.0$ K (Figure 4.2, (d-f)), and at

$\Delta T_{\text{sub}} \geq 3.5$ K (Figure 4.2, (g-j)).

The first group was characterized by the presence of elongated, faceted, blade-like crystals that seemed to decrease in length as subcooling increased. Similarly, the granular crystal habit became more evident with increasing ΔT_{sub} (Figure 4.2, (a-c)). A trigonal platelet with a concentric pattern can be seen embedded in the hydrate film at $\Delta T_{\text{sub}} = 1.5$ K (Figure 4.2, c).

The second region was dominated by a granular habit and individual granules decreased in size with the increasing ΔT_{sub}. Trigonal and hexagonal platelets were observed at 2.0, 2.5, and 3.0 K (Figure 4.2, (d-f)). In the third region, the hydrate film became smoother and darker. Individual granules became almost indistinguishable, although some individual euhedral crystals were still observed (Figure 4.2, (g-j)). In the third group, the individual euhedral crystals seemed to be mostly comprised of hexagonal platelets that became more circular in shape and smaller in diameter as subcooling increased. Table 4.1 summarizes the observed film morphologies.

Table 4.1: Grouping based on morphology for hydrate films formed with the y_{CH_4} = 0.90 gas mixture.

ΔT_{sub} /K	Crystal habit
≤ 1.5	Coarse, faceted with elongated crystals.
2.0−3.0	Granular. Single crystal granules noticeable
≥ 3.5	Smooth, polycrystalline. Individual crystallites not noticeable.

4.1.1.1.1 Single Crystals Figure 4.3 presents a summary of the observed habits of hydrate single crystals from the $y_{\text{CH}_4} = 0.90$ gas mixture. At $\Delta T_{\text{sub}} \leq 1.5$ K, the single-crystal habit was dominated by polyhedral platelets, growing from a preferred face in steps, marked by the appearance of "terraces" as they grew (Figure 4.3, (a-f)). With increasing subcooling, the blades and needle-like crystals widened, and their morphologies became platy (Figure 4.3, (g-j)). Although platy crystals were occasionally present at lower subcoolings, they only dominated the habit of single crystals above subcoolings of 1.5 K.

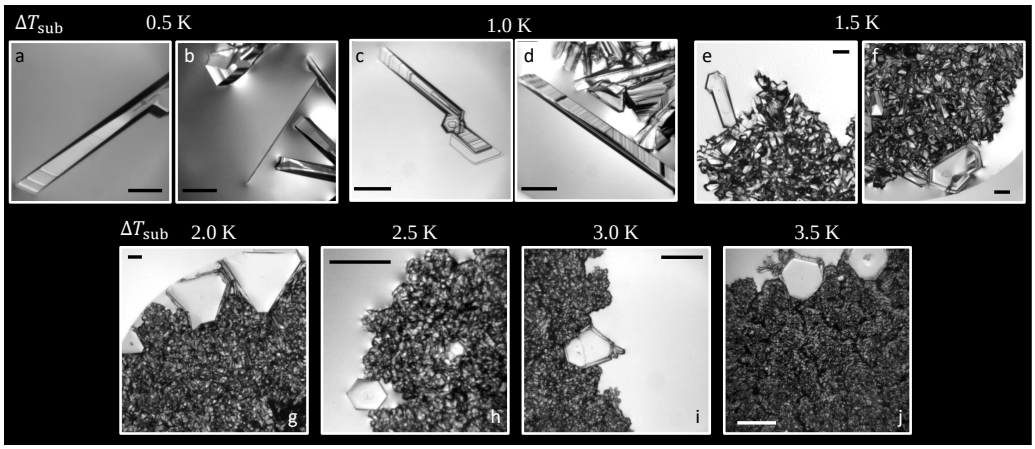

Figure 4.3: Characteristic habits of single crystals of methane + propane (y_{CH_4} = 0.90 gas mixture) hydrates. To facilitate viewing, magnification is slightly different for each image. Scale bars represent 250 μm. (a-j): P = 1.6 MPa. T_{HLV} = 283.02 K. (a, b): T = 282.52 K. (c, d): T = 282.02 K. (e, f): T = 281.52 K. (g): T = 281.02 K. (h): T = 280.52 K. (i): T = 280.02 K. (j): T = 279.52 K.

Trigonal platelets were the most common habit in the second morphology group of 2.0 K $\leq \Delta T_{sub} \leq$ 3.0 K (Figure 4.3, (g-i)), with occasional crystals exhibiting a hexagonal habit (Figure 4.3, (h). At higher subcoolings mostly hexagonal platelets were present (Figure 4.3, (j). Table 4.2 summarizes the groupings of single-crystal habit.

Table 4.2: Grouping based on morphology for single crystals formed with the y_{CH_4} = 0.90 gas mixture.

ΔT_{sub} /K	Crystal habit
$\leq$ 1.5	Elongated blades and platelets. Growth steps noticeable.
2.0 $-$ 3.0	Trigonal platelets. Hexagonal platelets present in lower numbers.
$\geq$ 3.0	Small, hexagonal platelets.

4.1.1.2 Constant Temperature Gradient

Figure 4.4 presents the morphology of the hydrate grown under a constant temperature gradient of 0.45 K·mm^{-1}, P = 0.7 MPa and T_{HLV} = 277.4 K. Crystal habit changed from coarse, elongated, faceted crystals at lower subcoolings, to a granular habit and to a smooth film with increasing subcooling. Three groups based on morphology were observed under gradient. Between 1.0 K $\leq \Delta T_{sub} \leq$

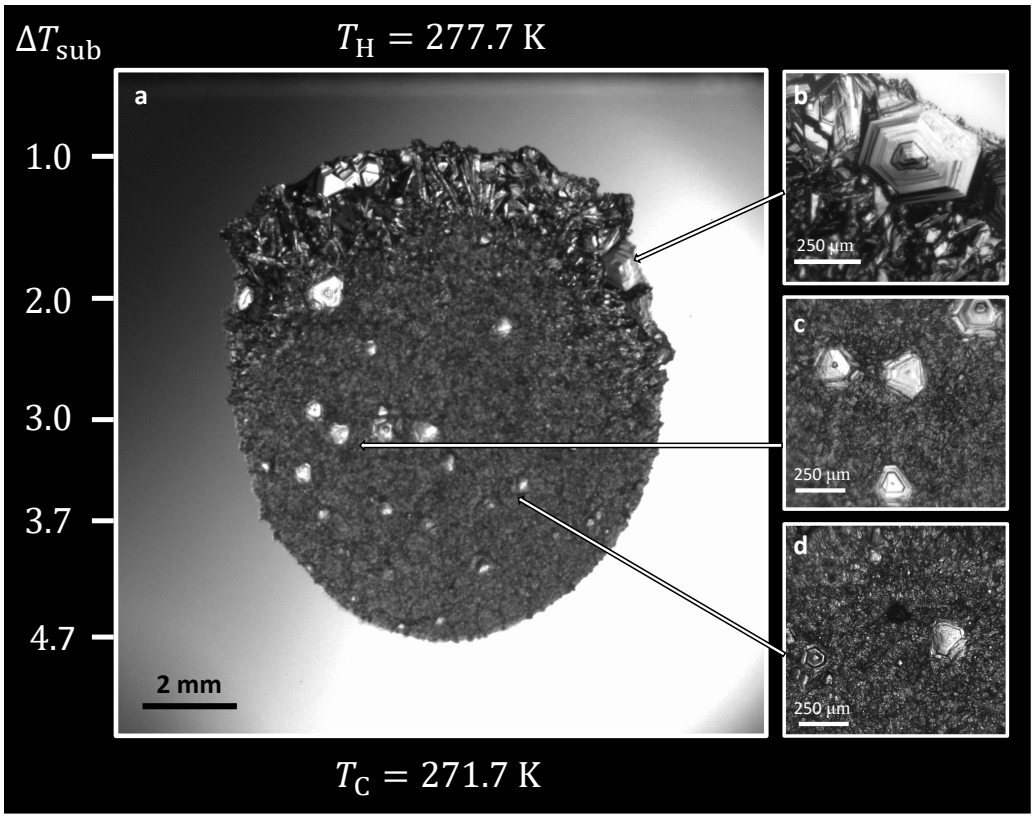

Figure 4.4: Methane + propane ($y_{CH_4} = 0.90$ gas mixture) hydrates formed under a constant temperature gradient of 0.45 K·mm^{-1}. $P = 0.7$ MPa. $T_{HLV} = 277.4$ K. (a) Bird's-eye view of the hydrate. (b-d) Magnified images of the crystal habit.

1.5 K, the first crystal habit could be observed (Figure 4.4, a). Elongated, faceted crystals dominated the morphology and gradually changed to a second granular habit at $\Delta T_{sub} \approx 2.0$ K. At $\Delta T_{sub} \geq 2.5$ K, the crystal habit became smoother, and no further sharp transition in morphology was observed (Figure 4.4, a).

Trigonal and hexagonal crystals were observed embedded in the hydrate film (Figure 4.4, (b-d)). Concentric patterns were observed in most of the single crystals (Figure 4.4, b). Single crystals seemed to be present mostly between 2.0 $\leq \Delta T_{sub} \leq 4.0$ K.

4.1.1.3 Growth Mechanism

Figure 4.5 shows a representative growth sequence for hydrates formed from the $y_{CH_4} = 0.90$ gas mixture, under uniform temperature. In general, the first crystal-

lites that grew in the liquid phase migrated towards the center of the droplet. The growth proceeded as a film with uniform morphology (Figure 4.5, (a-c)). Some of the single crystals that grew in the liquid film, away from the main film, became noticeable when they got engulfed by the hydrate film (Figure 4.5, (d-f)).

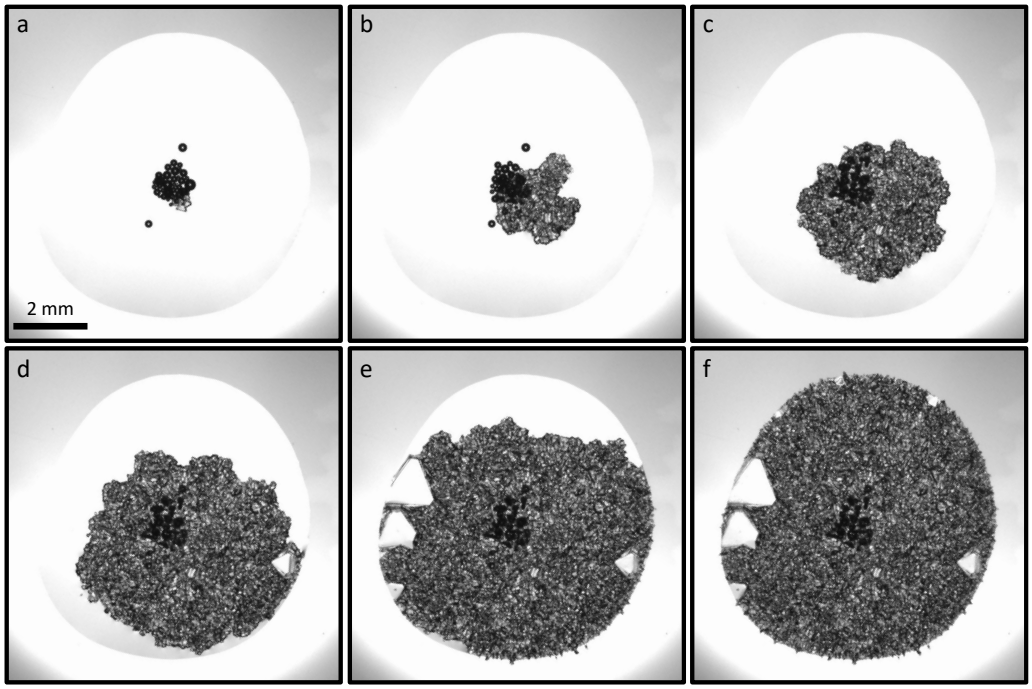

Figure 4.5: Growth sequence of methane + propane (y_{CH_4} = 0.90 gas mixture) hydrates, formed at uniform temperature. P = 1.6 MPa, T_{HLV} = 283.02 K, T = 281.02 K, ΔT_{sub} =2.0 K. (a), t = 1 min; (b), t = 2.3 min; (c), t = 3.6 min; (d), t = 4.9 min; (e), t = 6.2 min; (f), t = 8.7 min

Some of these crystals seemed to originate from detached shards of the main film. Figure 4.6-a shows the detachment of a crystal fragment from a fracture that appeared in the hydrate film. The fragment shows an elongated morphology, close to the dominant morphology in the film. The detached fragment remained close to the film interface but developed as a single crystal with a trigonal, platy morphology (Figure 4.6-(b-d)). The "seeding" fragments of single crystals grown through this mechanism could be observed in the center of the polyhedral habit (e.g., single crystals in Figure 4.4-(b-d)). Both the fracturing and detachment were observed at every studied subcooling. Details of partial dissociation and fracturing are presented in section 4.1.1.5.

Single, polyhedral crystals also grew independently, alongside the polycrys-

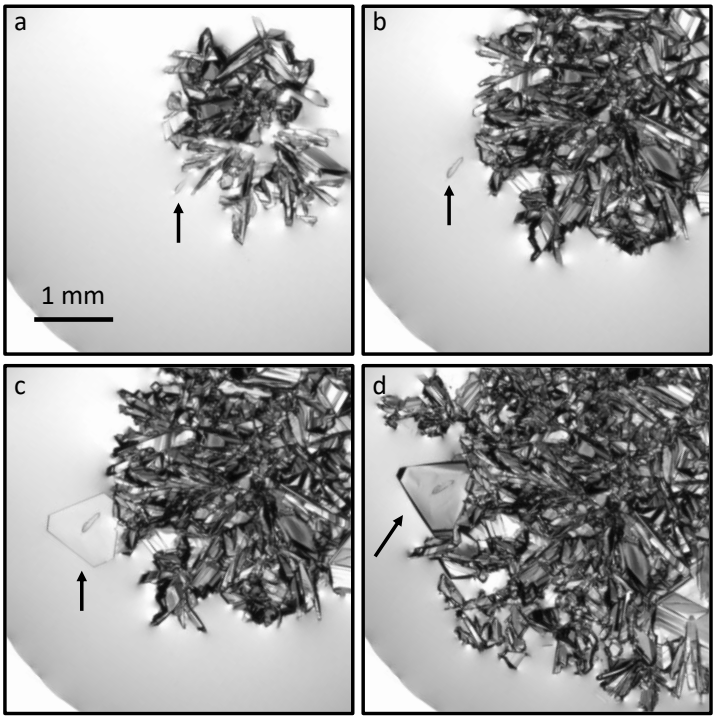

Figure 4.6: Methane + propane ($y_{\mathrm{CH_4}} = 0.90$ gas mixture) hydrates, formed under uniform temperature. $P = 1.6$ MPa, $T_{\mathrm{HLV}} = 283.02$ K, $T = 281.02$ K, $\Delta T_{\mathrm{sub}} = 1.0$ K. (a), partial dissociation of the growing film and a fracture appears in the hydrate film, leaving a detached fragment; (b), the fragment migrates towards the liquid phase close to the film; (c-d), a single trigonal platy crystal develops from the detached fragment.

talline film, and in the absence of shards (Figure 4.7-a). Single crystals, such as the ones shown in Figure 4.7-(a-b), grew in a concentric pattern. When some of the single crystals moved closer to the film (Figure 4.7-b), they attached to the film, and while some faces seemed to continue growing in steps, others continued to grow and fracture, producing flake-like crystallites (Figure 4.7-c, black arrow). The flaking continued from what seemed to be new steps, and these fragments appeared to populate the liquid phase surrounding the attached crystals (Figure 4.7-d). Growth from flakes proceeded with a morphology similar to that of the main film, filling the nearby spaces surrounding the single crystals (Figure 4.7-(e)). No further step-growth was observed on single crystals surrounded by the hydrate film (Figure 4.7-f). Growth beyond the attached crystals (Figure 4.7-f, blue line) proceeded with the same morphology as that of the main film

(Figure 4.7-f, red line)). Unattached crystals continued to grow under a stepped, two-dimensional nucleation mechanism (Figure 4.7-(a-f), gray arrows).

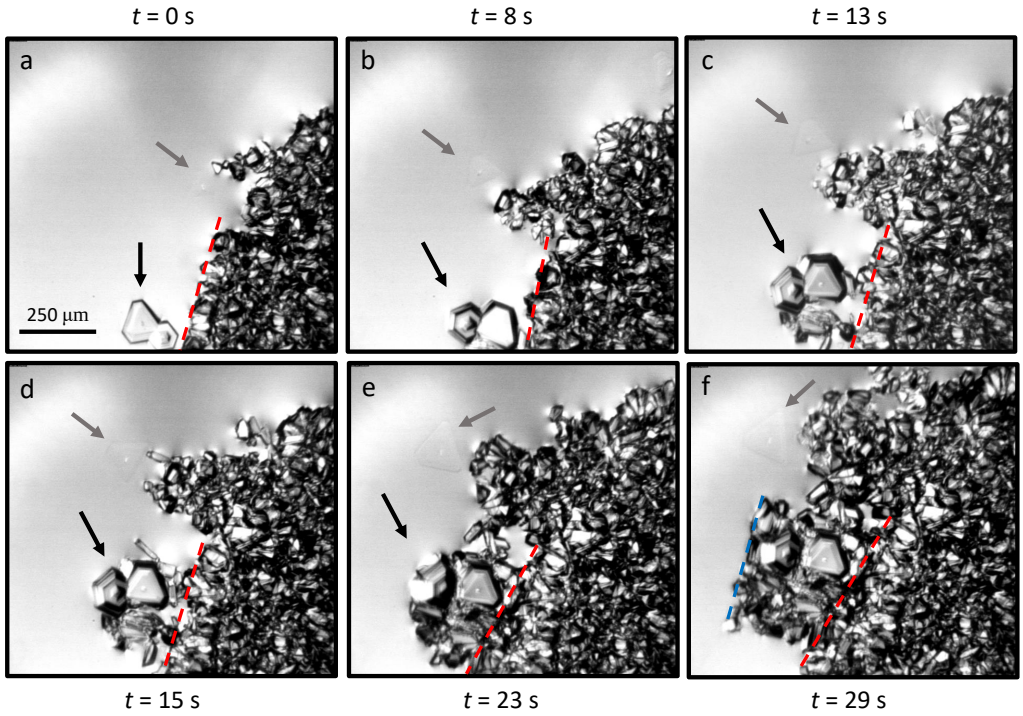

Figure 4.7: Methane + propane (y_{CH_4} = 0.90 gas mixture) hydrates formed at uniform temperature. P = 1.6 MPa, T_{HLV} = 283.02 K, T = 281.02 K, ΔT_{sub} = 2.0 K. Gray arrows: undisturbed single crystals; black arrows: single crystals after being disturbed by the hydrate film; dashed lines: apparent hydrate film fronts. (a), single crystals growing in a stepped mechanism (t = 0 s); (b), single crystals approaching the hydrate film (t = 8 s); (c), Single crystals attach to the hydrate film (black arrow), and some faces start to 'flake' while others grow in a new step (t = 13 s); (d), single crystals 'flaking' from the outermost step (black arrow) (t = 15 s); (e), 'flaking' continues at the hydrate-liquid interface (black arrow) (t = 23 s); (f), growth continues in a film-like fashion (blue line) beyond the single crystals and the original film (red line). (t = 29 s).

4.1.1.4 Ageing

Ageing of hydrates formed with the y_{CH_4} = 0.90 gas mixture, and maintained at constant T and P over a period of 12 h are presented in Figure 4.8. Some smoothening of the hydrate surface was observed, but no significant differences in

the overall morphology were seen.

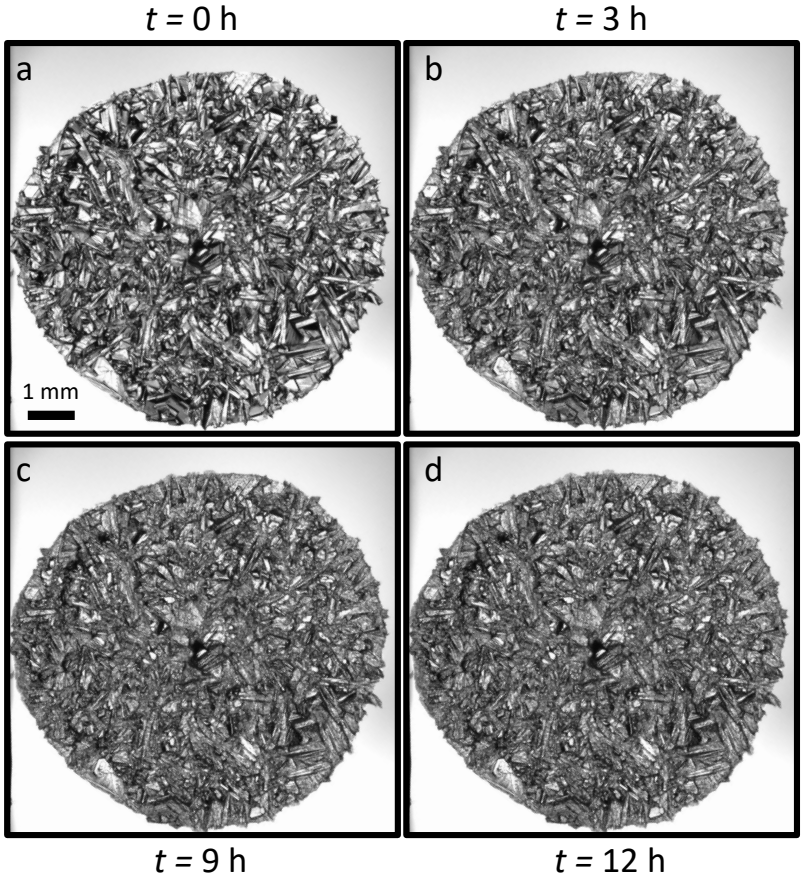

Figure 4.8: Ageing of methane + propane ($y_{CH_4} = 0.90$ gas mixture) hydrates. $P = 1.6$ MPa, $T_{HLV} = 283.02$ K, $T = 282.02$ K, $\Delta T_{sub} = 1.0$ K. Hydrate film at: a) $t = 0$ h. b) $t = 3$ h. c) $t = 9$ h. d) $t = 12$ h.

Under higher magnification and longer aging periods (30 hours), it was possible to observe more clearly the evolution of hydrates formed with the $y_{CH_4} = 0.90$ gas mixtures (Figure 4.9). A rougher texture on the faces of the polyhedral crystals was observed after 3 hours (Figure 4.9-b). After 18 h, the faces of the crystals became smoother with specks and indentations, and grain boundaries in the film became diffuse (Figure 4.9-c). After 30 h, grain boundaries and individual faces were no longer noticeable, and the film appeared dark (Figure 4.9-d).

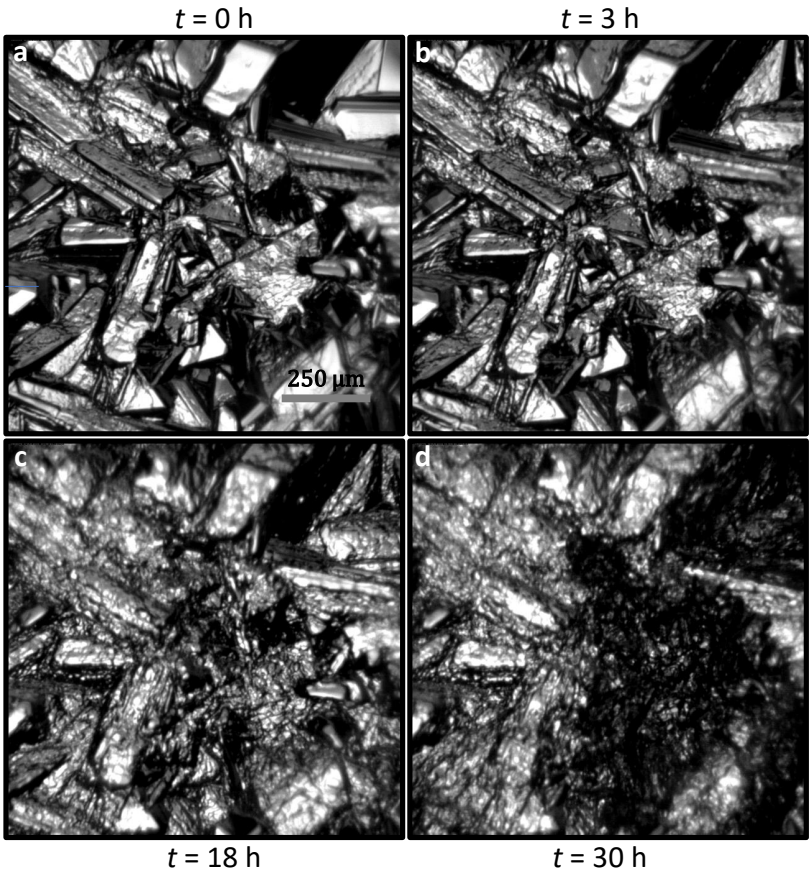

Figure 4.9: Ageing of methane + propane ($y_{CH_4} = 0.90$ gas mixture) hydrate. $P = 1.6$ MPa, $T_{HLV} = 283.02$ K, $T = 282.52$ K, $\Delta T_{sub} = 0.5$ K. Hydrate film at: a) $t = 0$ h. b) $t = 3$ h. c) $t = 18$ h. d) $t = 30$ h.

4.1.1.5 Dissociation and Regrowth

Regardless of the initial composition of the vapor phase or of subcooling, growth of the hydrate phase was always preceded by partial dissociation. Figure 4.10 shows the growth of hydrate crystals formed with the $y_{CH_4} = 0.90$ gas mixture under uniform temperature. As the hydrate film grew into the liquid phase, some crystals dissociated, creating a void in the film (Figure 4.10-(a-b)). Growth continued from the remaining crystals in contact with the liquid phase, and the fracture was covered again by hydrate (Figure 4.10-(c-d)). This mechanism was also observed with increasing subcooling, although the dissociation took place closer to the interface of the growing film.

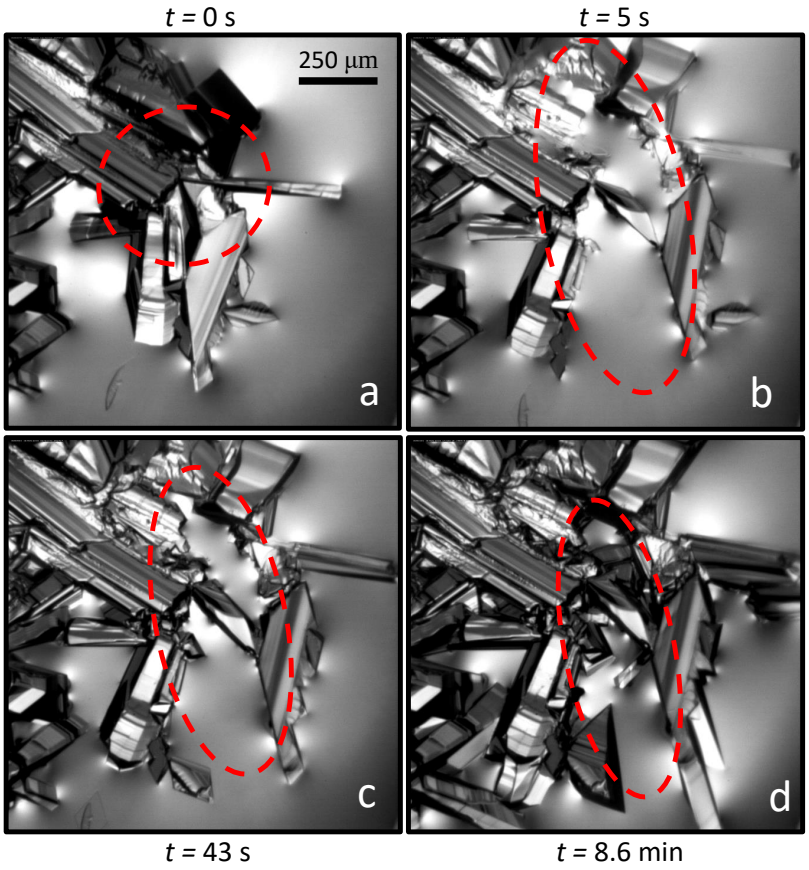

Figure 4.10: Methane + propane (y_{CH_4} = 0.90 gas mixture) hydrate growth at uniform temperature. P = 1.6 MPa, T = 282.52 K, T_{HLV} = 283.02 K, ΔT_{sub} = 0.5 K. a) Hydrate crystals growing (t = 0 s). b) Partial dissociation of crystals and fracture in the film (t = 5 s). c) Growth from the fractured and partially dissociated crystals (t = 43 s). d) Site of the fracture after growth (t = 8.6 min).

4.1.2 The methane + propane (y_{CH_4} = 0.98 mixture) system

4.1.2.1 Uniform surface temperature

Figure 4.11 shows the morphology of the (y_{CH_4} = 0.98 gas mixture) methane + propane hydrates, formed under uniform surface temperature and constant pressure. At $\Delta T_{sub} \leq 2.0$ K the original shape of the water droplet changed as liquid water was drawn towards the growing crystals. Elongated blade-like and acicular crystals were observed, as well as some platy crystals were present. The habit was significantly darker and smoother when $\Delta T_{sub} \geq 3.0$ K. At subcoolings of 4.0

K and 5.1 K (Figure 4.11, (d-e)), hydrates appeared entirely black. Significant spread of hydrate beyond the original boundaries of the droplet was observed. The halo covered almost the entire substrate when ΔT_{sub}= 5.1 K (Figure 4.11, e).

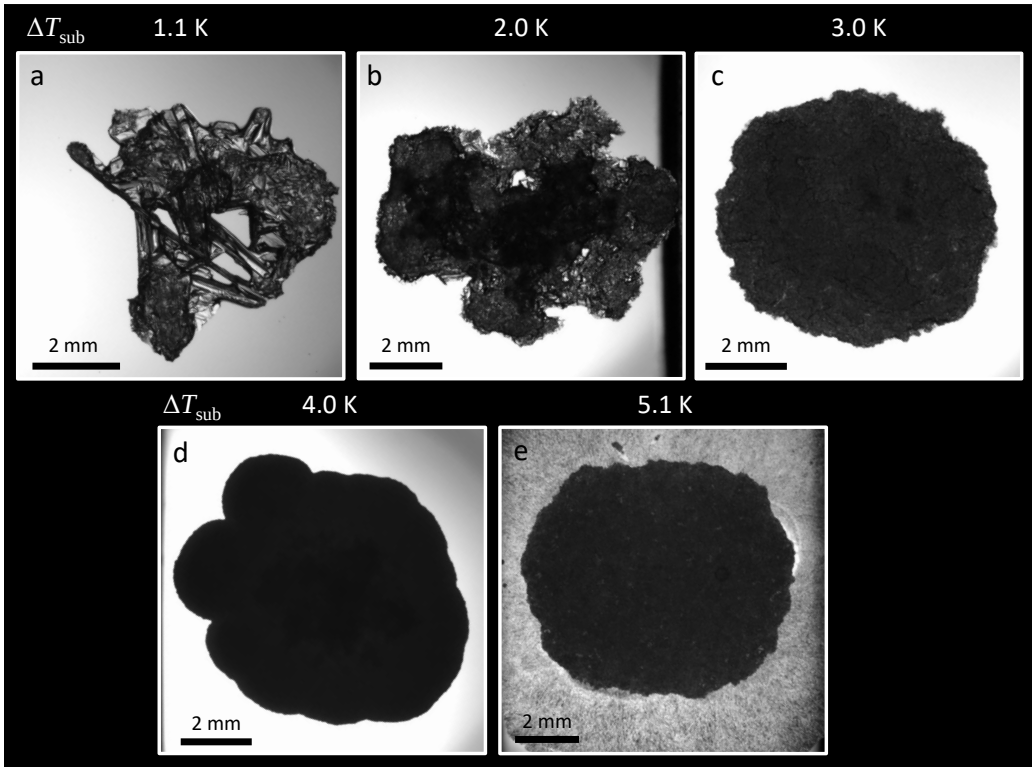

Figure 4.11: Morphology of methane + propane (y_{CH_4} = 0.98 gas mixture) hydrates formed under uniform surface temperature. (a-b): P = 1.5 MPa, T_{HLV} = 277.3 K. (c-e): P = 2.1 MPa, T_{HLV} = 280.5 K. (a), T = 276.24 K. (b), T = 275.24 K. (c), T = 277.5 K. (d), T = 276.5 K. (e), T = 275.4 K.

4.1.2.2 Constant temperature gradient

Figure 4.12 presents methane + propane hydrate formed with the y_{CH_4} = 0.98 gas mixture, under a constant temperature gradient of 0.45 K·mm^{-1} (P = 1.5 MPa, T_{HLV} = 277.3 K). The water droplet lost its shape as hydrate spread over the sapphire slide towards the lower temperature. This process seemed to draw the liquid water towards the hydrate film as the halo grew. Figure 4.12-a shows the hydrate film after complete coverage of the liquid surface. Transition from coarse to smooth hydrate habit was observed with increasing subcooling. Towards

lower subcoolings, big individual granules could be distinguished. Transition to a darker, smoother morphology was observed at a subcooling of approximately 2.2 K.

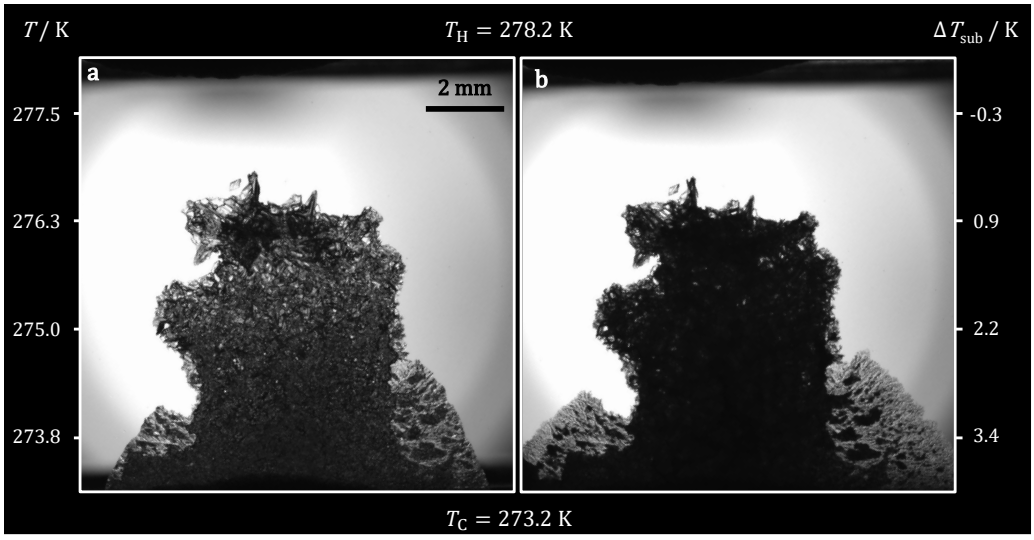

Figure 4.12: Methane + propane ($y_{CH_4} = 0.98$ gas mixture) hydrates formed under constant temperature gradient of 0.45 K·mm^{-1}. $P = 1.5$ MPa, $T_{HLV} = 277.3$ K. (a) Droplet covered with hydrate. (b) Hydrate 20 minutes after coverage of the droplet.

Towards higher subcoolings in Figure 4.12-a, a halo was observed to spread on the sapphire slide. The main hydrate film was dark and smooth, but the halo exhibited a gray, translucent habit. The halo was observed to have regions in which the morphology was darker and resembled that of the main hydrate film (Figure 4.12-a). Twenty minutes after complete coverage of the water surface, the hydrate crystals darkened to such an extent that it became impossible to clearly discern any details within the film (Figure 4.12-b).

4.1.2.3 Growth Mechanism

A hydrate formed with the $y_{CH_4} = 0.98$ gas mixture under uniform temperature is shown in Figure 4.13. The first hydrates to appear were dark and usually dissociated before growing into larger single crystals or a film (see section 4.1.1.5). Individual crystal growth was always preceded by partial dissociation. At $\Delta T_{sub} \leq 2.0$ K, the water droplet seemed to shrink (Figure 4.13-c). As crystals grew within the droplet, appreciable growth perpendicular to the sapphire slide was observed. Water was drawn towards the growing crystals, changing even further the shape

of the droplet (Figure 4.13-d). Hydrates became darker as time progressed (Figure 4.13-(e-f)).

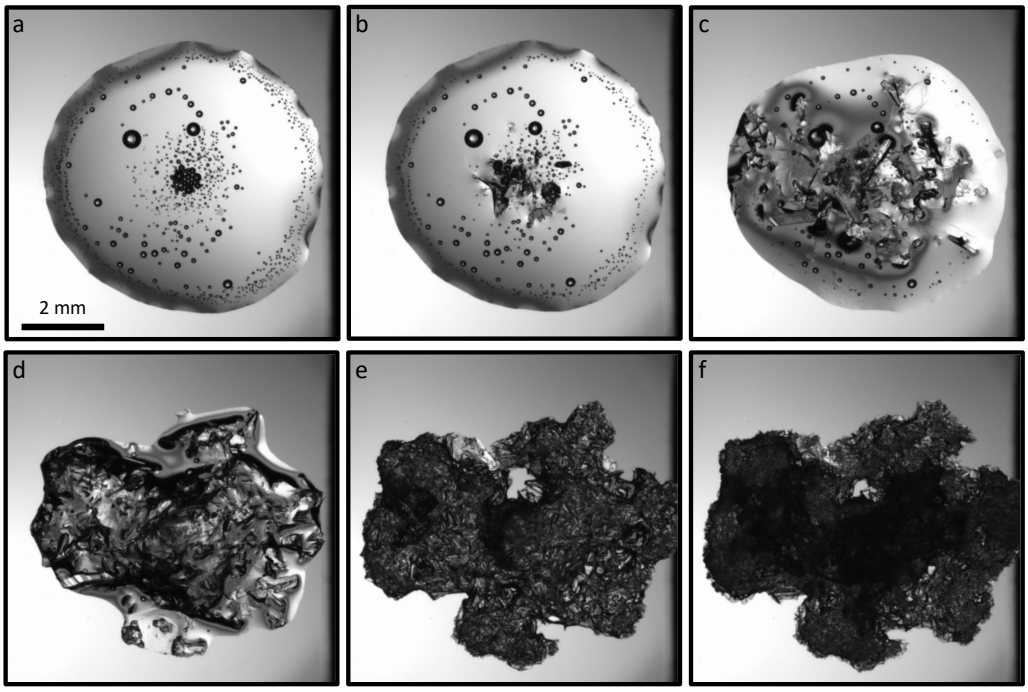

Figure 4.13: Growth of methane + propane ($y_{CH_4} = 0.98$ gas mixture) hydrates at uniform temperature. $P = 1.5$ MPa, $T_{HLV} = 277.3$ K, $T = 275.3$ K, ΔT_{sub} =2.0 K. (a) $t = 0$ h; (b), $t = 1.2$ h; (c), $t = 2.7$ h; (d), $t = 3.2$ h; (e), $t = 3.9$ h; (f), $t = 4.6$ h.

4.1.2.4 Ageing

Figure 4.14 shows ageing of hydrates formed with the $y_{CH_4} = 0.98$ gas mixture over 12 h. After two hours of ageing, most of the habit became darker, and most of the grain boundaries and crystal faces were no longer noticeable (Figure 4.14-b). As time progressed, the film habit became darker and the faces of some single crystals within the film developed a rough texture, with darker features on their faces (Figure 4.14(c-e)). After 12 h, most of the polycrystalline film appeared black. Only some portions of the polyhedral crystals preserved their shape and some resemblance to their original habit (Figure 4.14-d).

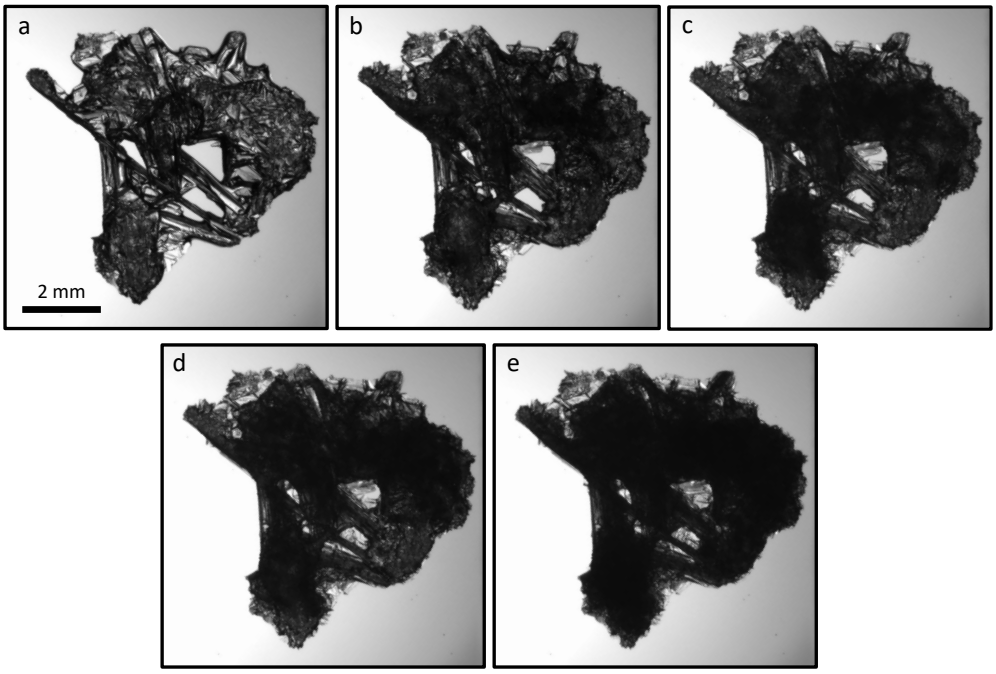

Figure 4.14: Ageing of methane + propane ($y_{CH_4} = 0.98$ gas mixture) gas hydrate. $P = 1.5$ MPa, $T_{HLV} = 277.3$ K, $T = 276.2$ K, $\Delta T_{sub} = 1.1$ K. Hydrate film at: (a), $t = 0$ h. (b), $t = 2$ h. (c) $t = 3$ h. (d), $t = 5$ h. (e), $t = 12$ h.

4.1.2.5 Dissociation and Regrowth

Figure 4.15 shows the partial dissociation and regrowth of hydrate formed with the $y_{CH_4} = 0.98$ gas mixture. Hydrate crystals can be seen dissociating on the areas denoted by yellow ellipses in Figure 4.15. Translucent crystallites resembling the original shape of the crystals can be seen after dissociation occurs. The frequency of the dissociation-regrowth events increased with increasing subcooling, but they were present at every studied subcooling.

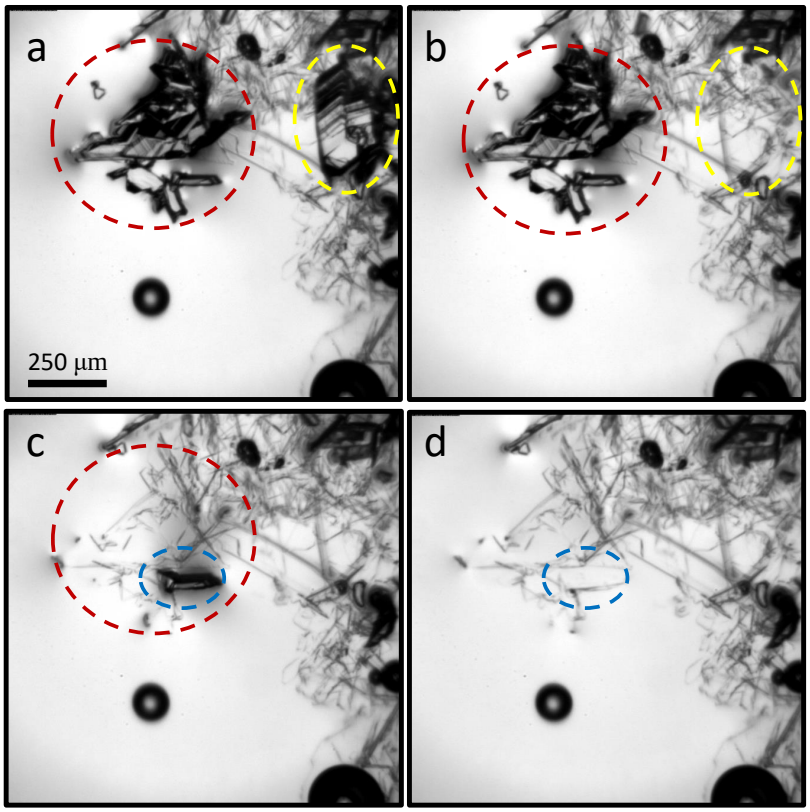

Figure 4.15: Methane + propane (y_{CH_4} = 0.98 gas mixture) hydrate growth at uniform temperature. P = 2.1 MPa, T = 278.5 K, T_{HLV} = 280.5 K, ΔT_{sub} = 2.0 K. (a) Dark crystals growing among light crystals (t = 0 s). (b) Partial dissociation of the crystal marked in yellow. (t = 1 s). (c) Partial dissociation of the crystal marked in red (t = 99 s). (d) Partial dissociation of the crystal marked in blue (t = 101 s).

4.2 Phase Equilibria

4.2.1 Controlled Dissociation

Figure 4.16-1 presents the controlled dissociation of hydrates formed from a y_{CH_4} = 0.90 gas mixture using a temperature gradient profile of 0.45 K·mm^{-1}. At each step, the observed hydrate-liquid interface appeared as a straight line (Figure 4.16-1, (b-d)). A 'band' appeared at the interface, on the hydrate film with every dissociation step (Figure 4.16-1, (b-d)). It was observed that the liquid phase preserved its shape throughout the dissociation procedure.

Hydrate dissociation using a gradient showed a different behavior for hydrates formed from the $y_{CH_4} = 0.98$ gas mixture (Figure 4.16-2). As the hydrate phase dissociated, the liquid phase was observed to move close to the interface and towards the cold side. As the liquid phase moved, hydrate was observed to grow on the slide, beyond the original boundary of the droplet, towards the cold side (T_c in Figure 4.16-2 (e-h)).

4.2.2 Hydrate-Liquid-Vapor Equilibrium Temperature

Hydrate-liquid-vapor equilibrium conditions were determined using the gradient dissociation method, as described in section 3.2.3. Figure 4.17 shows HLV equilibrium data on a pressure versus temperature diagram. The standard experimental uncertainties for the $y_{CH_4} = 0.90$ gas mixture were on average $u_{T_{exp}} = 0.14$ K and $u_{P_{exp}} = 0.005$ MPa.

For the $y_{CH_4} = 0.98$ gas mixture HLV equilibrium, standard experimental uncertainties were on average $u_{T_{exp}} = 0.21$ K and $u_{P_{exp}} = 0.005$ MPa. Table 4.3 presents the experimental uncertainties in this work, compared to the instrumental uncertainty.

Table 4.3: Experimental and instrumental standard uncertainties in this work

$10^2\ y_{CH_4}$	$u_{P_{exp}}$ / MPa	$u_{T_{exp}}$ / K	$u_{P_{inst}}$ / MPa	$u_{T_{inst}}$ / K
90	0.005	0.14	0.005	0.01
98	0.005	0.21		

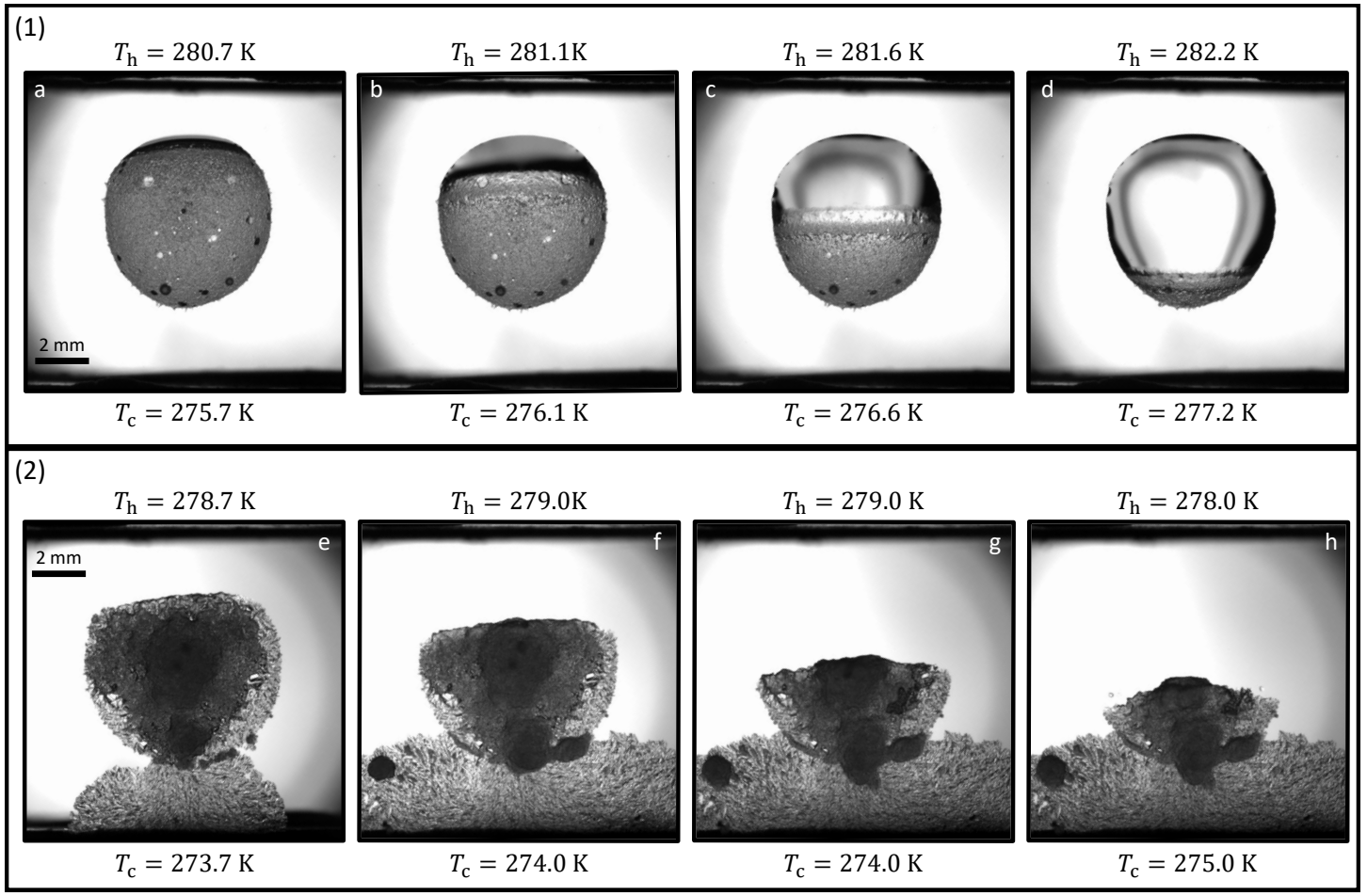

Figure 4.16: Stepwise dissociation sequences of methane + propane hydrates. (1): hydrates formed with the y_{CH_4} = 0.90 gas mixture, P = 0.9 MPa, T_{HLV} = 278.8 K; (a-d), The hydrate-liquid-vapor interface moves towards the cold side with increasing temperature steps. (2): hydrates formed with the y_{CH_4} = 0.98 gas mixture. P = 1.5 MPa, T_{HLV} = 277.3 K; (e-h), the liquid phase was drawn towards the cold side, leaving a small fraction at the interface.

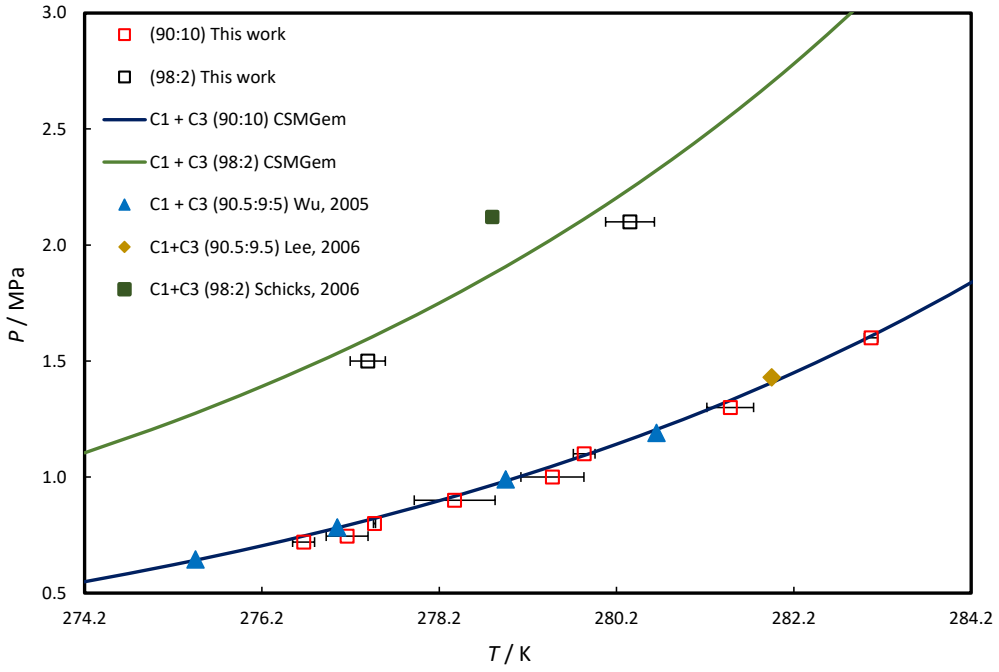

Figure 4.17: Hydrate-Liquid-Vapor equilibrium for the system methane + propane + water. □: $y_{CH_4} = 0.98$ gas mixture, $u_{T_{average}} = 0.21$ K; □, $y_{CH_4} = 0.90$ gas mixture, $u_{T_{average}} = 0.14$ K; ♦, data from Lee et al. (2006); ▲, data from Wu and Englezos (2006); ■; data from Schicks et al. (2006). Pressure standard experimental uncertainties are $u_P \leq 0.1$ MPa (not shown).

4.3 Kinetics

Figure 4.18 shows the hydrate-film growth velocity as a function of subcooling for hydrates formed from the $y_{CH_4} = 0.90$ gas mixture. Growth rates were observed to increase with increasing subcooling. The experimental standard uncertainty was on average $u_v = 3.16$ μm·s^{-1}.

The film growth velocities for the hydrates formed from the $y_{CH_4} = 0.98$ gas mixture could not be calculated. Due to the erratic crystal growth (section 4.1.2.3 and Figure 4.13), a well-defined growth vector could not be established for the $y_{CH_4} = 0.98$ gas mixture.

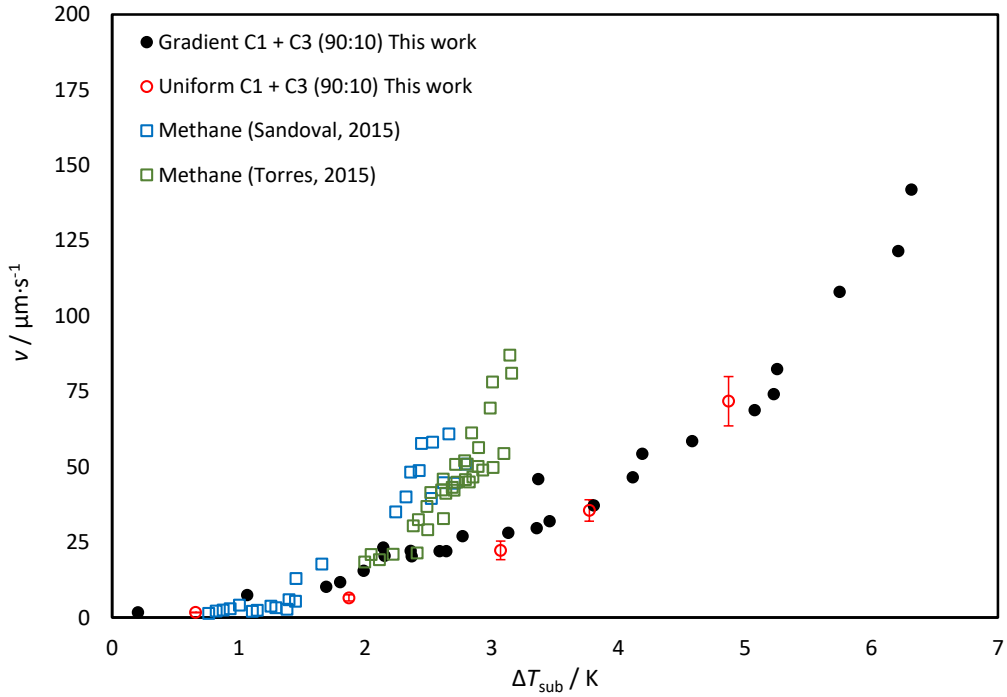

Figure 4.18: Hydrate-film growth rates as function of subcooling. ●, methane + propane (y_{CH_4} = 0.90 gas mixture) hydrates formed under constant temperature gradient (this work); ○, methane + propane (y_{CH_4} = 0.90 gas mixture) hydrates formed under uniform temperature, $u_{v_{average}}$ = 3.16 μm·s^{-1} (this work). □, pure methane formed under constant temperature gradient (Torres, 2015); □, pure methane hydrates formed under constant temperature gradient (Sandoval, 2015).

Chapter 5

Discussion

Methane + propane hydrate morphologies in this study were found to have a strong dependence on subcooling. The observed film morphologies were divided into three groups: (1) coarse, faceted films towards lower subcoolings; (2) granular and (3) smoother, polycrystalline films with increasing subcooling. Single crystals with polyhedral morphologies were observed to grow alongside hydrate films. These single crystals changed from elongated to rounded hexagonal platelets.

Growth rates were found to increase with increasing subcooling. Different growth mechanisms were observed on these systems, and some of the mechanisms seemed to change with increasing driving force. In this chapter, we explore some possible explanations for the observed phenomena.

5.1 Morphology

5.1.1 Hydrate film

Morphology of methane + propane hydrates was found to be very sensitive to subcooling. Increasing ΔT_{sub} led to finer, smoother films (Figure 4.1). This change in hydrate film habit is consistent with those reported for methane, propane, ethane, and mixtures of these hydrocarbons (Tanaka et al., 2009; Li et al., 2014; Peng et al., 2007; Lee et al., 2005).

The morphology of hydrate films formed from light hydrocarbons at high subcoolings has been often described as dendritic (Li et al., 2014; Smelik and King, 1997). In this work, films with larger grains observed at lower subcoolings changed to polycrystalline films at higher subcoolings (Figure 4.2-(f-j)). Granasy et al. (2004) have reported that crystalline materials change from single crystal to polycrystalline growth when growth front nucleation dominates the process. This process is also referred to as secondary nucleation (Makogon et al., 2007). When secondary nucleation is either absent or not the prevalent growth mechanism,

crystals develop dendritic morphologies at higher driving forces (Granasy et al., 2004). The films observed in this work seem to be dominated by a secondary nucleation mechanism at $\Delta T_{\text{sub}} \geq 3.0$ K, therefore a highly packed, polycrystalline film is observed instead of a dendritic film (Figure 4.1, Figure 4.2, Figure 4.4).

5.1.2 Growth and Habit of Single Crystals

Tanaka et al. (2009) have observed big polygonal crystals at lower subcoolings, and elongated, sword-like single crystals of smaller sizes with increasing driving force in methane, ethane, and propane hydrates. A similar trend was observed by Saito et al. (2011) on hydrates of methane + ethane + propane ternary mixtures, in which single crystals developed from polygonal to elongated polygonal and then to sword-like habits with increasing driving force. Lee et al. (2006) found methane + ethane polyhedral crystals growing in the liquid phase at lower subcoolings and developed a dendritic habit with increasing subcooling.

Single crystals of methane + propane hydrates formed with the $y_{\text{CH}_4} = 0.90$ gas mixture showed a different trend that those reported by Tanaka et al. (2009), Saito et al. (2011), and Lee et al. (2006). Habit was dominated by elongated, blade-like morphologies at lower subcoolings (Figure 4.3-(a-e)). With increasing subcooling, the habit changed to more uniform, platy crystals (Figure 4.3-(f-j)).

Nonetheless, a change from platy polyhedral crystals to elongated blade-like crystals with decreasing methane content can be observed in the results from (Saito et al., 2011) presented in Figure 5.1. Pure methane hydrates exhibit single crystals that are more symmetrical towards each face, whereas reducing the methane content increases the growth towards a preferred face, yielding elongated blade habits at the same subcooling. Habit of single crystals formed with the $y_{\text{CH}_4} = 0.90$ gas mixture at low subcoolings resembles the blades obtained by Saito et al. (2011) at higher methane + propane contents (Figure 5.1). The hexagonal platelets observed at higher subcoolings with the $y_{\text{CH}_4} = 0.90$ gas mixture, are more similar to the pure methane at lower subcoolings in Figure 5.1. This could indicate that as subcooling increases the habit of single crystals in the $y_{\text{CH}_4} = 0.90$ gas mixture is dominated by methane, and develop into platy morphologies.

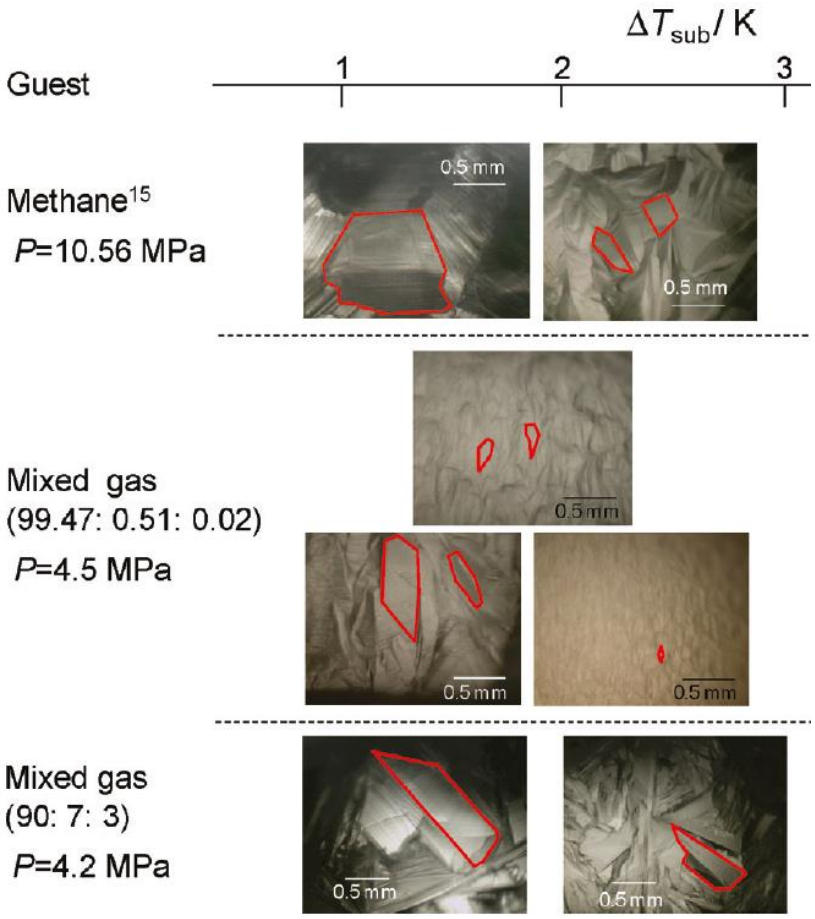

Figure 5.1: Crystal habit of methane + ethane + propane hydrates with respect to subcooling and gas composition. Modified from Saito et al. (2011).

Li et al. (2014) observed similar habits for single crystals formed with methane + ethane gas mixtures, like those observed in this work for hydrates formed with the $y_{CH_4} = 0.90$ gas mixture. Figure 5.2-a shows an elongated platy crystal, with noticeable growth steps in a methane + propane hydrate. Figure 5.2-b shows a methane + ethane hydrate platy crystal, growing in a preferred direction and in steps. These results provide visual evidence supporting the existence of different growth mechanisms for single crystals and hydrate films in mixed gas hydrates.

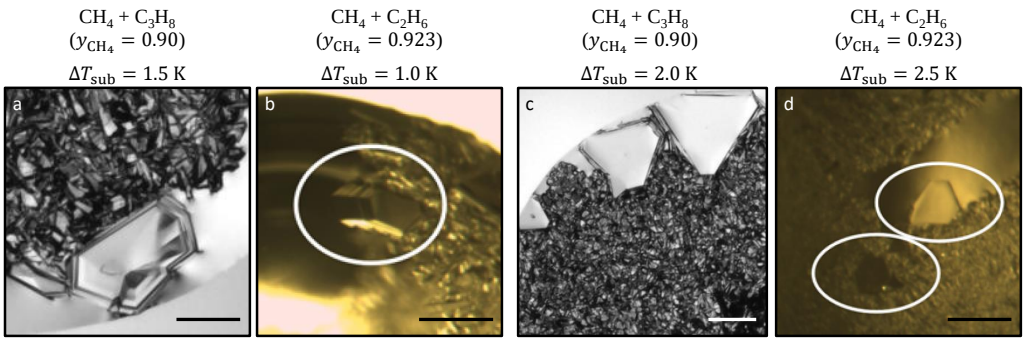

Figure 5.2: Comparison of single crystal habit between methane + propane and methane + ethane mixed hydrates. (a, c): methane + propane hydrates formed with a $y_{CH_4} = 0.90$ gas mixture (This work); (b, d): methane + ethane hydrates formed with a $y_{CH_4} = 0.923$ gas mixture. Modified from Li et al. (2014).

At higher subcoolings, trigonal, platy crystals were observed in (Figure 5.2-(c,d)). For these hydrates formed with methane + propane and methane + ethane gas mixtures, single crystals exhibited a different habit than that of the growing film. Nonetheless, the habit of the film is different for hydrates formed with the two mixtures. Methane + ethane hydrate films developed from leaf-like habits to dendritic with increasing subcooling (Li et al., 2014) (Figure 5.2-(b, d)), whereas the film formed with the methane + propane mixture is granular for 1.5 K $< \Delta T_{sub} \leq$ 3.0 K, with decreasing grain size with increasing subcooling (Figure 5.2-(a, c); Figure 4.2-(c-f)). Furthermore, at $\Delta T_{sub} \geq$ 3.5 K (Figure 4.2-(e-f)), the hydrate film formed with the $y_{CH_4} = 0.90$ gas mixture resembles a spherulitic, polycrystalline growth, rather than a dendritic habit.

5.1.2.1 Single crystal formation

Li et al. (2014) hypothesized that the appearance of big, single crystals alongside the main hydrate film could be due to coexistence of sI and sII hydrates. Higher enclathration rates of ethane compared to propane in the hydrate film could lead to higher local concentrations of methane near the film, causing the growth of methane-dominated sI single crystal structures (Li et al., 2014). Higher enclathration rates have been reported for propane in methane + propane mixed hydrates (Klapproth et al., 2019; Uchida et al., 2004; de Menezes et al., 2019; Kini et al., 2004). It could be possible that higher propane consumption near the growing hydrate film could lead to higher methane concentration in the liquid phase and the formation of the polyhedral morphologies.

Li et al. (2014) has proposed that large crystals are indicative of sI formation in the methane+ethane system. Pure methane experiments with the same apparatus

used in this work (Duquesnay et al., 2016) also show these large crystals. Thus, it seems plausible that the large crystals observed with methane + propane mixtures in this work are also sI (Figure 4.3).

5.1.2.2 Detachment

Big crystals seem to form in two ways. Some crystals grew from fragments that detached from the main hydrate film Figure 4.6, while others were only noticed after their growth was disturbed and were incorporated by the hydrate film (Figure 4.5-(e-f)). The origin of the big crystals can be inferred from their morphologies: those formed from detachment usually exhibit a 'seed' with the habit of their 'mother' fragments in the center of the crystal (Figure 4.6, Figure 4.3, Figure 4.2-(d)), whereas those that grew independently were completely translucent (Figure 4.5-(e-f)).

The detached fragments bear the elongated habit of the hydrate film, but the resulting crystal has the habit of a platy crystal (Figure 4.6). This could indicate a change to two-dimensional nucleation, layer-by-layer mechanism. This could also be due to spatial restrictions in the film, compared to the crystals growing independently in the liquid phase. This change in the growth and morphology of the detached fragments was observed in the range 0.5 K $\leq \Delta T_{\text{sub}} \leq$ 4.0 K (Figure 4.6). At $\Delta T_{\text{sub}} >$ 4.0 K these changes are not noticeable, due to the fast growth of the hydrate film.

Completely translucent crystals could be formed from detached fragments that are too small to be observed. It is also possible that these crystals are formed by secondary nucleation in the liquid film, away from the main hydrate film. This phenomenon occurs more frequently as driving force increases since the energy barrier for growth is lower than that of nucleation (Makogon et al., 2007; Sunagawa, 2005). This could explain in part the observed increase in the number of single crystals with increasing ΔT_{sub}. Finally, these crystals could originate from crystallites in the liquid phase that remained after dissociation at the beginning of each cycle.

5.1.2.3 Attachment and "flaking"

Single crystals growing in the liquid phase were observed to attach to the growing hydrate film and change their subsequent morphology (Figure 4.7). The concentric steps that appear as the single crystals grow are a clear indication of a two-dimensional, layer-by-layer mechanism (Figure 4.7-(a-c)) (Chernov, 1984). The hydrate film in Figure 4.7 grew with a different mechanism and developed a different morphology than the single crystals. Remains of flakes from this process can be observed around the faces of polyhedral crystals embedded in the film at different subcoolings (Figure 5.3).

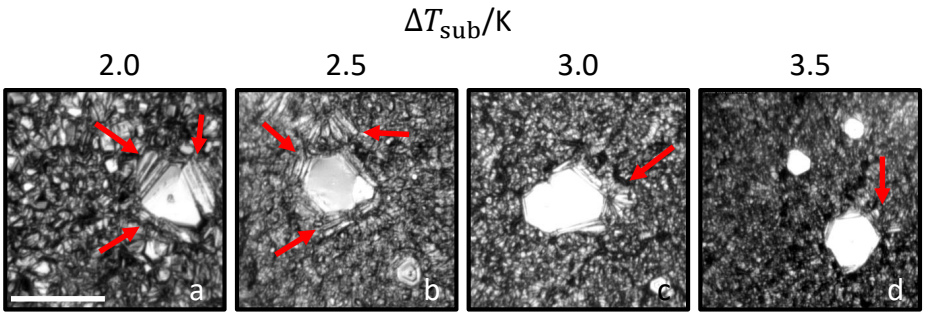

Figure 5.3: Methane + propane ($y_{CH_4} = 0.90$ gas mixture) hydrate single crystals embedded in the film at different subcoolings. Red arrows indicate the remains of the flaking process. Scale bar is 250 μm.

The onset of flaking could be due to a disruption of the growing step of the single crystals. Step growth requires smooth, ordered surfaces, whereas adhesive-type and polycrystalline growth are characterized by surface roughness (Sunagawa, 2005; Mullin, 2001; Granasy et al., 2004). When the smooth surface of the polyhedral crystals attaches to the hydrate film, the latter could induce defects in the growing surface of the crystal (Figure 4.7-(b-c)). Subsequently, those defects could cause roughness and a more disordered growth, that leads to flaking of the crystal face.

This analysis is supported by the observation of flaking in faces that are not in direct contact with the hydrate film. After attachment, the highly-ordered step is no longer stable, once one of its faces is disrupted by the film, and other faces start to flake (Figure 4.7-(b-e), black arrows). Furthermore, the developing of flakes, and the film-like growth arising from them occurs before the main hydrate film incorporates the attached crystals (Figure 4.7-f, red line). This could indicate that the mechanism by which the hydrate film grows is induced in the single crystals by creating rough faces that will no longer grow in steps.

The changes in morphology caused by the attachment of single crystals to the film and the detachment of crystallites from the film are evidence of different mechanisms dominating the growth of single crystals and hydrate films.

5.1.2.4 Step-growth mechanism

In most of the polyhedral single crystals observed in the present study, a pattern of concentric steps was observed in their habits (Figure 4.4, (b-d); Figure 4.2-c; Figure 4.3-(a,c,d)). At low driving forces, the spiral mechanism is expected to dominate the crystal growth (Sunagawa, 2005; Mullin, 2001). Although the patterns observed in single crystals of methane + propane hydrates in this work

are concentric, spirals are not obvious.

Figure 5.4-a shows the characteristic morphology of a crystal growing in a spiral mechanism (Mullin, 2001). Figure 5.4-b shows the morphology of crystals grown in a layer-by-layer mechanism. The steps in the layer-by-layer mechanism are created by successive two-dimensional growth when the growth rates are higher than in the spiral mechanism (Chernov, 1984). The single crystals in this work (e.g., Figure 5.4-c) exhibited growth patterns that closely resemble that of layer-by-layer, two-dimensional nucleation mechanism (Figure 5.4-b). This indicates that this layer-by-layer, two-dimensional growth is the dominant mechanism for single crystal growth in the studied methane + propane hydrates.

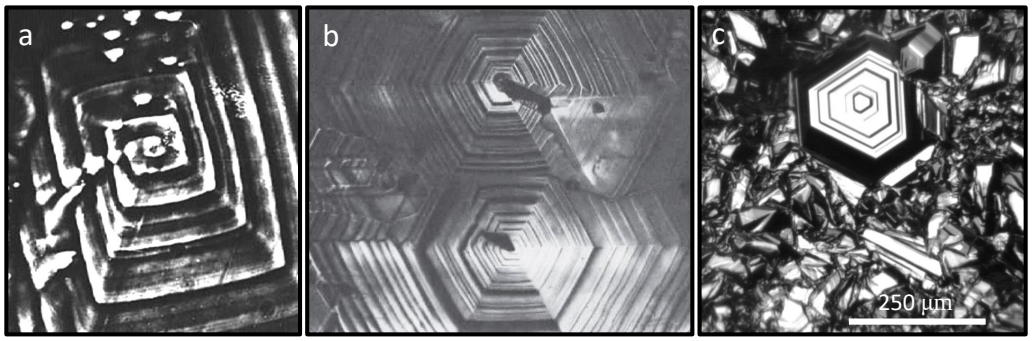

Figure 5.4: Comparison of crystal habits with concentric and spiral patterns. (a), spiral pattern in a crystal face (modified from Mullin (2001)); (b), concentric steps in crystals (modified from Chernov (1984)); (c), Concentric steps in a methane + propane single crystal formed from a $y_{CH_4} = 0.90$ gas mixture (this work).

Step growth was observed on single crystals through a wide range of subcoolings (Figure 4.3), even though the layer-by-layer mechanism is only expected to occur at lower subcoolings (Mullin, 2001; Sunagawa, 2005; Chernov, 1984). This could explain the lower growth rates observed for single crystals compared to that of hydrate films.

5.1.3 Growth rates and changes in crystal habit

The growth rates of individual crystals formed from the $y_{CH_4} = 0.90$ gas mixture were measured and compared to the hydrate film growth rates (Figure 5.5).

The smallest crystals that could be resolved using the optical instruments are approximately 2.5 - 5.0 μm across. By setting 5.0 μm·s^{-1} as the lower bound for uncertainty in the growth rates of single crystals, it seems that the growth rates between the film and the single crystals become significantly different at $\Delta T_{sub} \approx$ 2.5 K (Figure 5.5, (1d)). At $\Delta T_{sub} > 3.0$ K, single crystals could only be observed

after being incorporated into the crystal film, and their growth rates were not measured.

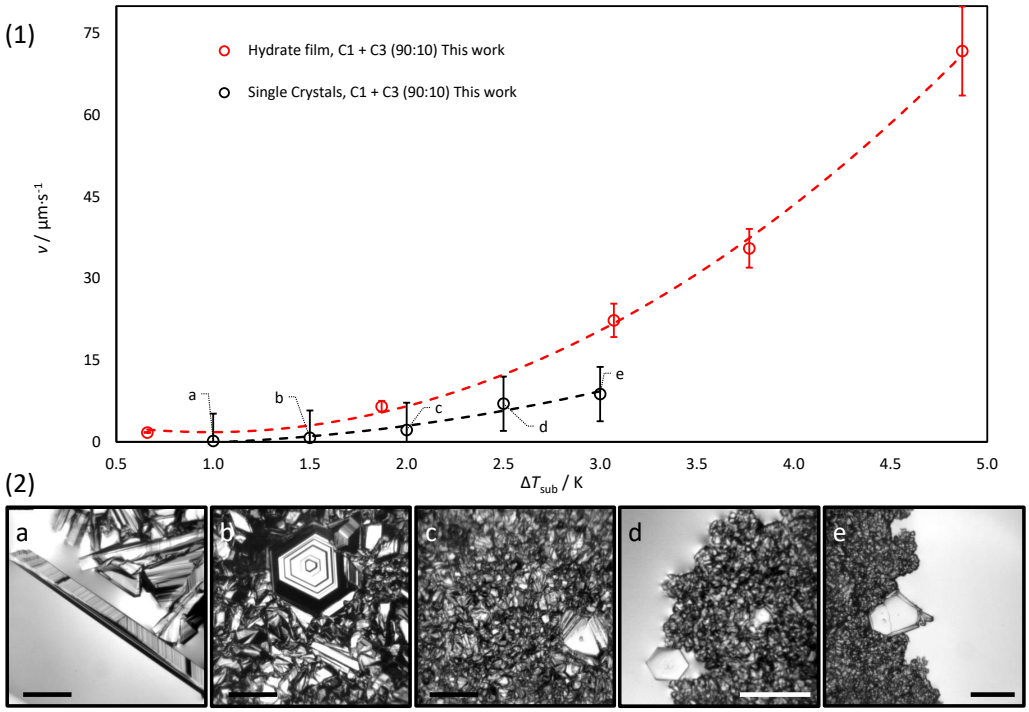

Figure 5.5: Changes in growth rates and habit for single crystals, formed with a $y_{CH_4} = 0.90$ gas mixture, as function of subcooling. (1): growth rates as function of subcooling; ○, hydrate film; ○, single crystals; red error bars: standard experimental uncertainty; black error bars: $u_v = 5.0$ μm·s^{-1}; data labels, reference to habits presented in (2). Dashed curves are presented for better readability of the figure and do not represent a modeling effort. (2): representative crystal habit at the same subcooling as ○ in (1); a, $\Delta T_{sub} = 1.0$ K; b, $\Delta T_{sub} = 1.5$ K; c, $\Delta T_{sub} = 2.0$ K; d, $\Delta T_{sub} = 2.5$ K; e, $\Delta T_{sub} = 3.0$ K. Scale bars represent 250 μm.

When growth rates are close between the film and the single crystals, their growth mechanisms are similar, therefore their habits are also similar (Figure 5.5-2(a-c)). As driving force increases, so does the difference between growth rates, and the morphologies became more dissimilar.

It is known that there is a tight relationship between driving force, growth mechanism, and crystal habit (Sunagawa, 2005; Mullin, 2001; Chernov, 1984). Growth rates for single crystals are less sensitive to subcooling than those of the hydrate film (Figure 5.5), which could help explain why polyhedral crystals

could be observed at higher driving forces, although they are expected only at low driving forces (Sunagawa, 2005; Mullin, 2001).

5.1.3.1 Change in hydrate film growth mechanism

The hypothesized transition from a growth-dominated to a secondary nucleation-dominated regime (Li et al., 2014; Granasy et al., 2004) appears to occur at $\Delta T_{\text{sub}} \approx 2.5$ K (Figure 5.5). This is consistent with the changes observed in the crystal habit. At $\Delta T_{\text{sub}} \leq 2.0$ K, where film and single-crystal growth rates are the closest, the habit of polyhedral crystals resemble that of the hydrate film (Figure 5.5-2(a-c)). At $\Delta T_{\text{sub}} \approx 2.5$ K, where trends in growth rates for the film and single crystals seem to diverge, the habit of the film is comprised of small, individual crystal grains (Figure 5.5-2(d)). At $\Delta T_{\text{sub}} = 3.0$ K, where the growth rates for the film are higher than for single crystals, the hydrate film appears to have a smooth polycrystalline habit, noticeably different from that of polyhedral crystals (Figure 5.5-2(e)). Grouping according to velocities corresponds closely to groupings according to morphology, as shown in Table 5.1.

Table 5.1: Grouping based on morphology compared to grouping based on growth rates of single crystals.

Grouping	On habit ΔT_{sub} /K	On growth rates ΔT_{sub} /K	Film habit	Single crystal habit
1	≤ 1.5	≤ 2.0	Coarse, faceted with elongated crystals.	Elongated blade-like and elongated platy.
2	2.0−3.0	2.0-2.5	Granular, single crystal granules noticeable.	Trigonal and hexagonal platelets.
3	≥ 3.5	≥ 3.0	Smooth, polycrystalline. Individual crystallites not noticeable.	Small, rounded hexagonal platelets.

5.1.4 Dissociation and Regrowth

Hydrates from methane + propane $y_{CH_4} = 0.90$ and $y_{CH_4} = 0.98$ gas mixtures exhibited partial dissociation of the growing crystals. New hydrates filled the space left by partial dissociation, supporting the continued growth of the hydrate film (Figure 4.10 and Figure 4.15). The fact that dissociation and regrowth were observed in the two mixtures and at every subcooling suggests that it could be a phenomenon characteristic to hydrate crystal growth from methane + propane mixtures.

5.1.4.1 Local heterogeneities hypothesis

It has been reported that growing methane + propane hydrates consume propane at a higher rate than that of propane and its concentration in the hydrate phase is greater than in the liquid and vapor phases (Kini et al., 2004; Klapproth et al., 2019; Uchida and Kawabata, 1996). This depletion of propane from the liquid phase could lead to heterogeneities arising from local concentration gradients around the growing mixed + propane crystals. This anisotropy could lead to the dissolution of the guest molecules back to the liquid phase, causing some crystals to dissociate. After this process, enclathration could be once again favorable, and growth occurs in the region close to the dissociation event.

5.1.4.2 Metastable phases hypothesis

Hydrates formed from methane-rich methane + propane mixtures have been observed to form sI alongside the expected sII structure (Klapproth et al., 2019; Schicks et al., 2006; de Menezes et al., 2019; Uchida et al., 2004). This coexistence of polymorphs is attributed to the rapid enclathration of propane. The appearance of metastable sI structures observed in mixtures with the same composition as those used in the present work (de Menezes et al., 2019; Klapproth et al., 2019), could be the cause of the dissociation events, as these structures transform into the most stable sII phase. This hypothesis is also supported by visual observations of polymorph transformations in methane and methane + propane hydrates, found in literature: the crystals dissociate and regrow into the new hydrate phases (Schicks and Ripmeester, 2004; Schicks et al., 2006). The dissociation and growth observed in this work could be caused by metastable sI hydrates, formed after propane depletion in the liquid phase, which transform into the most stable sII over time. A similar hypothesis to explain differences in morphology between single crystals and hydrate film of methane + ethane is presented by Li et al. (2014).

According to the Ostwald's rule of step, the first solid phase to appear in crystallization processes is not necessarily the most stable, but the one which leads to the less change in energy (Mullin, 2001). The formation of metastable

hydrate structures due to energy minimization and subsequent transformation into most stable structures could explain the dissociation and growth.

5.1.5 Temperature Gradient

Morphology of hydrates formed under a constant temperature gradient was presented in Figure 4.4. The hydrate film changes from a coarser, faceted habit to a granular and smoother film with increasing subcooling. This result is consistent with the changes observed in uniform surface temperature experiments (Figure 4.1 and Figure 4.2). Morphology transition could be observed at $\Delta T_{\text{sub}} \approx 2.0$ K in Figure 4.4. This transition is consistent with the grouping based on morphology presented in subsubsection 4.1.1.1. Most importantly, this supports the hypothesized transition in the film growth mechanism found at $\Delta T_{\text{sub}} \approx 2.5$ K (subsection 5.1.3).

The gradient formation method allowed to identify the main characteristics of methane + propane hydrate habit. The morphology trends observed in several uniform temperature experiments could be observed using a single gradient experiment (Figure 4.4).

5.1.6 Ageing

In methane + propane ($y_{\text{CH}_4} = 0.90$ gas mixture) hydrates aged under constant temperature and pressure the grain boundaries became diffuse, and the surface became more uniform and darker (Figure 4.9). Methane hydrates have been also observed to become more uniform and darker over time (Beltran and Servio, 2010; Sandoval, 2015).

The crystalline solid phase has a tendency to reach a minimum surface energy and their particle size distribution will naturally become narrower over time (Mullin, 2001). Metastable polymorphs are also expected to transform to more stable phases over time, leading to changes in habit of the crystal phase (Sunagawa, 2005; Mullin, 2001). Metastable hydrate phases have been observed to form in methane + propane hydrates, formed with similar compositions to those in this work (Schicks et al., 2006; Klapproth et al., 2019; de Menezes et al., 2019). It is possible that a combination of both phenomena (surface energy minimization combined with the transformation of metastable phases) are responsible for the observed ageing behavior.

5.1.7 The methane + propane ($y_{\text{CH}_4} = 0.98$ gas mixture) system

Figure 5.6 shows changes in crystal habit for hydrates formed with the $y_{\text{CH}_4} = 0.98$ gas mixture superimposed to the phase equilibria measured by Schicks et al. (2006) for this system. Red cross markers in Figure 5.6-(1) represent the experimental

conditions. It can be seen that the conditions in the present work are away from the polymorph transition points observed by Schicks et al. (2006) (× in Figure 5.6-1).

It can be concluded that the observed changes in morphology for this system are kinetic in nature and not thermodynamic, since the hydrates were formed in a region where polymorph transformations are not expected. Furthermore, ageing of hydrates from this mixture showed a darker habit after a 12-hour lapse, which also points to a kinetic phenomenon Figure 4.14.

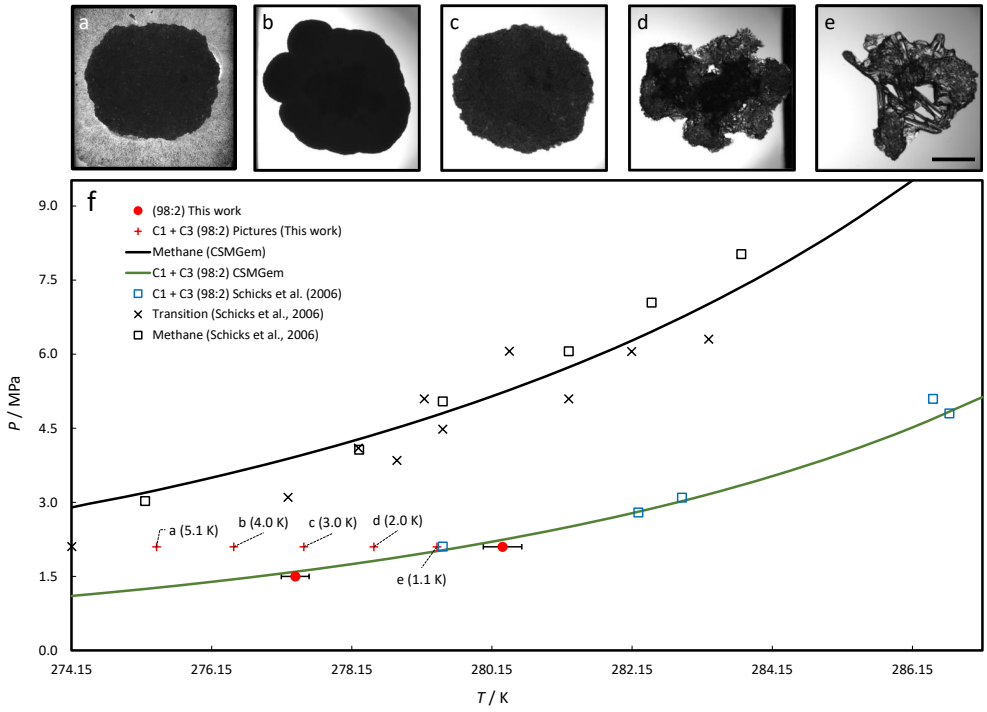

Figure 5.6: Habit of methane + propane mixed hydrates with respect to subcooling on a PT partial phase diagram and compared to data from Schicks et al. (2006). (a-b): hydrates formed with a $y_{CH_4} = 0.98$ gas mixture, under uniform temperature at $P = 2.1$ MPa; scale bar represent 2 mm (this work). (f): partial phase diagram; (—, —), CSMGem software hydrate-liquid-vapor equilibrium predictions; (□), methane (Schicks et al., 2006); (×), transition points from sII to sI + sII (Schicks et al., 2006);(□), methane + propane ($y_{CH_4} = 0.98$ gas mixture) (Schicks et al., 2006); (●), methane + propane ($y_{CH_4} = 0.98$ gas mixture) (this work); (+), crystallization conditions for methane + propane mixed hydrates formed from a $y_{CH_4} = 0.98$ gas mixture (legends indicate corresponding insert and subcooling; this work).

5.2 Phase Equilibria

As shown in Figure 4.17 and subsection 4.2.2, standard experimental uncertainties were on average 0.14 K for the system containing the $y_{CH_4} = 0.90$ gas mixture, and 0.21 K for the system with the $y_{CH_4} = 0.98$ gas mixture. For the $y_{CH_4} = 0.90$ gas mixture, some standard experimental uncertainties were as low as the instrumental uncertainty.

The results for the $y_{CH_4} = 0.90$ gas mixture agree within uncertainty (Figure 4.17) to literature data (Wu and Englezos, 2006; Lee et al., 2006) and specialized software (Sloan and Koh, 2008a) for hydrate-liquid-vapor equilibrium calculations. In the system containing the $y_{CH_4} = 0.98$ gas mixture, measured T_{HLV} was higher than the CSMGem software predictions Figure 4.17. Hydrate-liquid-vapor equilibrium reported by Schicks et al. (2006) also seems to deviate from the software prediction, although towards lower temperatures (Figure 4.17).

5.2.1 Controlled hydrate dissociation

The directional dissociation of hydrates using a temperature gradient showed two different behaviors for the methane + propane mixtures studied. For the hydrates from the $y_{CH_4} = 0.90$ gas mixture, the shape of the droplet was preserved after each dissociation step (Figure 4.16-1). Dissociation of hydrates formed with the $y_{CH_4} = 0.98$ gas mixture was characterized by the formation of halo towards the cold side of the slide, and the retraction of the remaining liquid phase with each dissociation step (Figure 4.16-2).

The bands observed at the hydrate-liquid-vapor interface at each dissociation step in hydrates from the $y_{CH_4} = 0.90$ gas mixture (Figure 4.16) have also been observed for the controlled dissociation of methane + carbon dioxide mixed hydrates (Ortiz, 2017). The formation of these bands could be caused by partial dissociation of hydrates beyond the interface, followed by a reformation of the hydrate film into a stable interface. Ortiz (2017) found that the presence of these bands in the dissociation of methane + carbon dioxide hydrates does not affect on the measured hydrate-liquid-vapor equilibrium temperatures. It has been reported different coexisting structures and metastable phases in hydrates formed using this particular mixture (de Menezes et al., 2019; Schicks et al., 2006). Metastability could be responsible for the formation of the bands in gradient dissociation.

The observed contraction of the liquid phase in methane + propane hydrates formed with the $y_{CH_4} = 0.98$ gas mixture has also been observed in dissociation experiments of carbon dioxide and methane + carbon dioxide mixtures (Sandoval, 2015; Ortiz, 2017).

5.3 Kinetics

The technique allowed to obtain reproducible measurements of the hydrate film growth rates for methane + propane hydrates formed from a $y_{CH_4} = 0.90$ gas mixture. The standard experimental uncertainty was $u_v = 3.16$ μm·s^{-1}. Uncertainties increased with increasing subcooling. This could be attributed to the faster growth rates observed at these subcoolings, which make it more difficult to measure the growing film (Figure 4.18). Gradient formation experiments offer representative values of film growth rates, which agree with the uniform temperature measurements.

At $\Delta T_{sub} \leq 2.5$ K, there seemed to be no significant differences in the growth rates of methane + propane hydrates formed with the $y_{CH_4} = 0.90$ gas mixture, compared to those of methane hydrates (Sandoval, 2015; Torres, 2015) (Figure 4.18). At $\Delta T_{sub} \geq 2.5$ K, growth rates for the methane + propane hydrates were lower than those of methane hydrates (Figure 4.18).

These results are in agreement with other studies, that found lower hydrate film growth rates for hydrates formed with mixtures of methane with other hydrocarbons (Peng et al., 2007; Saito et al., 2011; Li et al., 2014). Propane hydrates have been shown to have the slowest hydrate growth rates compared to methane and ethane (Tanaka et al., 2009). Furthermore, mixtures of methane + ethane + propane and methane + propane have also been observed to have the slowest growth rates, compared to systems without propane (Saito et al., 2011; Peng et al., 2007). This observation could be due to the lower solubility of propane in water, compared to that of methane and ethane at the same temperature (Sloan and Koh, 2008a).

As seen in Figure 4.18, the 3-in-1 technique allowed to measure hydrate film growth rates under several subcoolings with a single gradient experiment. This reduced considerably the number of experiments and experimental times. If a region of interest is identified using a gradient, uniform temperature experiments can be used to obtain the growth rates at the desired ΔT_{sub}.

In the case of methane + propane hydrates formed from the $y_{CH_4} = 0.98$ gas mixture, the hydrate film growth rate could not be calculated using the same procedure as the hydrates formed with the $y_{CH_4} = 0.90$ gas mixture. As shown in Figure 4.5-2, the growth of hydrates formed with the $y_{CH_4} = 0.98$ gas mixture was erratic and did not allow to establish clear growth rate vectors.

Chapter 6

Conclusions

The objective of this work was to evaluate the suitability of the 3-in-1 technique to the study the morphology and growth mechanisms, phase equilibria, and kinetics of gas hydrates from methane + propane mixtures. The technique allowed to provide insights on the complex mechanisms governing hydrate crystallization and morphological features, while allowing to measure the conditions and rates at which they form.

Morphology of methane + propane hydrates is divided into single-crystal habit and film habit. The habit between the two became different with increasing subcooling. This difference is attributed to changes in growth rates between single crystals and hydrate films with increasing subcooling. The transition between the two mechanisms seems to be at $\Delta T_{\text{sub}} \approx 2.5$ K, observed as the point at which growth rates became significantly higher for films than that of single crystals.

Although gas hydrate films are often observed to develop into dendritic morphologies with increasing ΔT_{sub}, those reported in this work develop into granular and polycrystalline morphologies. This is explained by growth front nucleation dominating the growth of hydrate films at $\Delta T_{\text{sub}} \geq 3.0$ K.

Some platy crystals grew from detached fragments from the hydrate film, and growth from single crystals that came into contact with the film adopted its growth mechanism and habit. These results point out to a difference in growth mechanism between the film and the single platy crystals observed to grow in the liquid phase.

Hydrate growth was found to be preceded by partial dissociation of the hydrate crystals. This could be due to heterogeneities in the hydrate-liquid interface or the transformation of initial metastable phases as growth proceeds.

Phase equilibria conditions for the studied systems were determined with uncertainties of $u_T = 0.14$ K for the $y_{\text{CH}_4} = 0.90$ gas mixture, and $u_T = 0.21$ K for the $y_{\text{CH}_4} = 0.98$ gas mixture. Pressure uncertainties were on average as low as the instrumental uncertainty. Hydrate film growth rates were measured with an un-

certainty of $u_v = 3.16\ \mu\text{m}\cdot\text{s}^{-1}$. Nonetheless, a clear film growth vector is required to establish the growth rates. The growth mechanism observed in hydrates from the $y_{\text{CH}_4} = 0.98$ gas mixture did not allow to establish the growth rates.

Overall, the 3-in-1 technique proved to be a versatile tool in the study of hydrates from binary mixtures of methane + propane, allowing to retrieve reproducible growth rates, equilibrium temperatures and morphological features in a fraction of the time of traditional techniques. Furthermore, the complex mechanisms by which mixed hydrates grow were observed using the technique, and are valuable information to expand our understanding of these systems.

6.1 Recommendations for future work

- Using spectroscopic techniques, such as Raman spectroscopy, could help to establish if the observed dissociation and regrowth of hydrate crystals is due to polymorphs transforming to their most stable structure. The Raman spectra of the crystals before and after the dissociation events should be able to identify differences in crystalline structure and guest occupancy.

- Thermal imaging of the growing hydrates would provide additional information on heterogeneities that might occur during hydrate growth, and their role in the observed dissociation and regrowth of hydrate crystals.

- The hydrates formed with the $y_{\text{CH}_4} = 0.98$ gas mixture proved to have complex growth mechanisms. Although, the expected structure transitions and the corresponding changes in morphology could not be observed in the present work. Experiments at higher subcoolings could provide visual evidence of the transformation process.

  - Forming hydrate under constant temperature gradient, within the subcoolings at which transformations are expected, could help to identify the subcooling at which they occur.
  - To identify if habit changes are kinetic in nature or structure transformations, hydrate could be formed at low subcoolings and aged, and then brought to higher subcoolings. If a different change in morphology occurs, compared to that of ageing, could indicate that the change in morphology is due to a change in crystalline structure.

- On the growth of single crystals, it would be valuable to change the subcooling conditions as they grow. This could help to identify the onset of a different growth mechanism, marked by a change in the crystal habit.

Bibliography

Ballard, A. and Sloan, E. (2001). Hydrate phase diagrams for methane + ethane + propane mixtures. *Chemical Engineering Science*, 56(24):6883–6895.

Beltran, J. and Servio, P. (2008). Equilibrium studies for the system methane + carbon dioxide + neohexane + water. *Journal of Chemical Engineering Data*, 53:1745–1749.

Beltran, J. and Servio, P. (2010). Morphological investigations of methane-hydrate films formed on a glass surface. *Journal of Crystal Growth and Design*, 10:4339–4347.

Beltran, J. G., Bruusgaard, H., and Servio, P. (2012). Gas hydrate phase equilibria measurement techniques and phase rule considerations. *The Journal of Chemical Thermodynamics*.

Chernov, A. A. (1984). *Modern Crystallography III*. Springer Berlin Heidelberg, 1 edition.

Chu, C.-K., Lin, S.-T., Chen, Y.-P., Chen, P.-C., and Chen, L.-J. (2016). Chain length effect of ionic liquid 1-alkyl-3-methylimidazolium chloride on the phase equilibrium of methane hydrate. *Fluid Phase Equilibria*, 413:57–64.

Davies, S. R., Hester, K. C., Lachance, J. W., Koh, C. A., and Sloan, E. D. (2009). Studies of hydrate nucleation with high pressure differential scanning calorimetry. *Chemical Engineering Science*, 64(2):370–375.

Davy, H. (1811). The bakerian lecture: On some of the combinations of oxymuriatic gas and oxygene, and on the chemical relations of these principles, to inflammable bodies. *Philossophical Transactions of the Royal Society of London*, 101:1–35.

de Menezes, D. É. S., Sum, A. K., Desmedt, A., de Alcântara Pessôa Filho, P., and Fuentes, M. D. R. (2019). Coexistence of sI and sII in methane-propane hydrate former systems at high pressures. *Chemical Engineering Science*, 208:115149.

DuQuensay, J. R., Diaz, M. C., and Beltran, J. G. (2016). Novel gas hydrate reactor design: 3-in-1 assessment of phase equilibria, morphology and kinetics. *Fluid Phase Equilibria*, 413.

Duquesnay, J., Diaz Posada, M., and Beltran, J. (2016). Novel gas hydrate reactor design: 3-in-1 assessment of phase equilibria, morphology and kinetics. *Fluid Phase Equilibria*, 413:148–157.

DuQuesnay, J. R. (2014). A novel apparatus design, experimental methods and validation for temperature controlled directional crystallization of high-pressure gas hydrate systems. mathesis, Royal Military College of Canada, Kingston, ON, Canada.

Englezos, P. (1993). Clathrate hydrates. *Industrial & Engineering Chemistry Research*, 32:1251–1274.

Englezos, P., Kalogerakis, N., Dholabhai, P. D., and Bishnoi, P. R. (1987). Kinetics of formation of methane and ethane gas hydrates. *Chemical Engineering Science*, 42:2647–2658.

Englezos, P. and Ngan, Y. T. (1994). Effect of polyethylene oxide on gas hydrate phase equilibria. *Fluid phase equilibria*, 92:271–288.

Esmail, S. and Beltran, J. (2016). Methane hydrate propagation on surfaces of varying wettability. *Journal of Natural Gas Science and Engineering*, 35:1535–1543.

Fleyfel, F., Song, K. Y., Kook, A., Martin, R., and Kobayashi, R. (1993). Interpretation of carbon-13 NMR of methane/propane hydrates in the metastable/nonequilibrium region. *The Journal of Physical Chemistry*, 97(25):6722–6725.

Freer, E. M., Selim, M. S., and Sloan, E. D. (2001). Methane hydrate film growth kinetics. *Fluid phase equilibria*, 185:65–75.

Granasy, L., Pusztai, T., Borzsony, T., Warren, J., and Douglas, J. (2004). A general mechanism of polycrystalline growth. *Nature Materials*, 3:645–650.

Granasy, L., Pusztai, T., G., T., Warren, J., and Douglas, J. (2005). Growth and form of spherulites. *Physical Review E*, 72:011605.

Hammerschmidt, E. G. (1934). Formation of gas hydrates in natural gas transmission lines. *Industrial and Engineering Chemistry Fundamentals*, 26:851–855.

Hu, Y., Lee, B. R., and Sum, A. K. (2017). Insight into increased stability of methane hydrates at high pressure from phase equilibrium data and molecular structure. *Fluid Phase Equilibria*, 450:24–29.

Kelland, M. A. (2006). History of the development of low dosage hydrate inhibitors. *Energy & Fuels*, 20(3).

Kini, R. A., Dec, S. F., and Sloan, E. D. (2004). Methane + propane structure II hydrate formation kinetics. *The Journal of Physical Chemistry A*, 108(44):9550–9556.

Klapproth, A., Piltz, R. O., Kennedy, S. J., and Kozielski, K. A. (2019). Kinetics of si and mixed si/sii, gas hydrate growth for a methane/propane mixture using neutron diffraction. *The Journal of Physical Chemistry C*, 123(5):2703–2715.

Koh, C. A., Sloan, E. D., Sum, A. K., and Wu, D. T. (2011). Fundamentals and applications of gas hydrates. *Annu. Rev. Chem. Biomol. Eng*, 2:237–257.

Kumar, N. (2016). A 3-in-1 approach to evaluate gas hydrate inhibitors. mathesis, Royal Military College of Canada.

Kumar, N., Chowdhury, N. B., and Beltran, J. G. (2019). A 3-in-1 approach to evaluate gas hydrate inhibitors. *Energies*, 12(15):2921.

Larsen, R., Knight, C., and Sloan, D. (1998). Clathrate hydrate growth and inhibition. *Fluid Phase Equilibria*, 150-151:353–360.

Lee, J., Susilo, R., and Englezos, P. (2005). Methane-ethane and methane-propane hydrate formation and decomposition on water droplets. *Chemical Engineering Science*, 60:4203–4212.

Lee, J. D., Song, M., Susilo, R., and Englezos, P. (2006). Dynamics of methane-propane clathrate hydrate crystal growth from liquid water with or without the presence ofn-heptane. *Crystal Growth & Design*, 6(6):1428–1439.

Lee, S., Kim, H., and Lee, J. (2014). Morphology study of methane–propane clathrate hydrates on the bubble surface in the presence of sds or pvcap. *Journal of Crystal Growth*, 402:249–259.

Li, S., Sun, C., Liu, B., Li, B., Chen, G., and Sum, A. (2014). New observations and insights into the morphology and growth kinetics of hydrate film. *Scientific Reports*, 4:4129.

Makogon, Y. F. (1965). Hydrate formation in the gas-bearing beds under permafrost conditions. (english translation). *Gazovaia Promyshlennost*, 56:14–15.

Makogon, Y. F., Melikhov, I. V., Kozlovskaya, E. D., and Bozhevol'nov, V. E. (2007). Secondary nucleation in the formation of methane crystal hydrate. *Russian Journal of Physical Chemistry A*, 81(10):1645.

Mei, D.-H., Liao, J., Yang, J.-T., and Guo, T.-M. (1996). Experimental and modeling studies on the hydrate formation of a methane + nitrogen gas mixture in the presence of aqueous electrolyte solutions. *Industrial & Engineering Chemistry Research*, 35(11):4342–4347.

Mullin, J. W. (2001). *Crystallization*. Elsevier.

Natarajan, V., Bishnoi, P. R., and Kalogerakis, N. (1994). Induction phenomena in gas hydrate nucleation. *Chemical Engineering Science*, 49(13):2075–2087.

Ohmura, R., Matsuda, S., Itoh, S., Ebinuma, T., and Narita, H. (2005a). Formation and growth of structure-h hydrate crystals on a water droplet in contact with methane gas and a large-molecules guest substance liquid. *Crystal Growth and Design*, 5:1821–1824.

Ohmura, R., Matsuda, S., Uchida, T., Ebinuma, T., and Narita, H. (2005b). Clathrate hydrate crystal growth in liquid water saturated with a guest substance: Observations in a methane + water system. *Crystal Growth and Design*, 5:953–957.

Ohmura, R., Shimada, W., Uchida, T., Mori, Y., Takeya, S., Nagao, J., Minagawa, H., Ebinuma, T., and Narita, H. (2004). Clathrate hydrate crystal growth in liquid water saturated with a hydrate-forming subtance: variations in crystal morphology. *Philosophical Magazine*, 84:1–16.

Ortiz, N. (2017). 3-in-1 technique applied to mixed ch4 + co2 gas hydrates. Undergraduate thesis, Universidad de los Andes & Royal Military College of Canada, Kingston, ON, Canada.

Ovalle, S., Martinez, C., Bonilla, L., Lara, A., and Beltran, J. G. (2019). Assessment of commercial hydrate inhibitors using the 3-in-1 method. *The Canadian Journal of Chemical Engineering*, 97(11):2818–2826.

Peng, B., Dandekar, A., Sun, C., Luo, H., Ma, Q., Pang, W., and Chen, G. (2007). Hydrate film growth on the surface of a gas bubble suspended in water. *Journal of Physical Chemistry B*, 111:12485–12493.

Ripmeester, J. A., Tse, J. S., Ratcliff, C. I., and Powell, B. M. (1987). A new clathrate hydrate structure. *Nature*, 325:135–136.

Saito, K.and Kishimoto, M., Tanaka, R., and Ohmura, R. (2011). Crystal gorwth of clathrate hydrate at the interface between hydrocarbon gas mixture and liquid water. *Crystal Growth and Design*, 11:295–301.

Sandoval, J. F. (2015). A comparative study on the growth mechanism, kinetics and morphology of carbon dioxide and methane hydrates. Undergraduate thesis, Universidad de los Andes & Royal Military College of Canada, Kingston, ON, Canada.

Santen, R. A. V. (1984). The ostwald step rule. *The Journal of Physical Chemistry*, 88(24):5768–5769.

Schicks, J. M. and Luzi-Helbing, M. (2013). Cage occupancy and structural changes during hydrate formation from initial stages to resulting hydrate phase. *Spectrochimica Acta Part A: Molecular and Biomolecular Spectroscopy*, 115:528–536.

Schicks, J. M., Naumann, R., Erzinger, J., Hester, K. C., Koh, C. A., and Sloan, E. D. (2006). Phase transitions in mixed gas hydrates: experimental observations versus calculated data. *The Journal of Physical Chemistry B*, 110(23):11468–11474.

Schicks, J. M. and Ripmeester, J. A. (2004). The coexistence of two different methane hydrate phases under moderate pressure and temperature conditions: Kinetic versus thermodynamic products. *Angewandte Chemie International Edition*, 43:3310–3313.

Servio, P. and Englezos, P. (2003). Morphology of methane and carbon dioxide hydrates formed from water droplets. *AIChE Journal*, 49:269–276.

Sloan, E. (2004). Introductory overview: Hydrate knowledge development. *American Mineralogist*, 89:1155–1161.

Sloan, E. D. (2003). Fundamental principles and applications of natural gas hydrates. *Nature*, 426:353–359.

Sloan, E. D., Koh, C., Sum, A. K., Ballard, A. L., Creek, J., Eaton, M., Jason, L., McMullen, N., Palermo, T., Shoup, G., and Larry, T. (2011). *Hydrates In Flow Assurance*. Elsevier.

Sloan, E. D. and Koh, C. A. (2008a). *Clathrate Hydrates of Natural Gases*. Chemical Industries. CRC Press, 3rd edition.

Sloan, E. D. and Koh, C. A. (2008b). *Clathrate Hydrates of Natural Gases*. CRC Press.

Smelik, E. A. and King, H. E. (1997). Crystal-growth studies of natural gas clathrate hydrates using a pressurizes optical cell. *American Mineralogist*, 82:88–98.

Smith, J., H., V. N., and M., A. (2001). *Introduction to Chemical Engineering Thermodynamics*. McGraw-Hill.

Sun, C. Y., Z., P. B., Dandekar, A., Ma, Q. L., and J., C. G. (2010). Studies on hydrate film growth. *Annual Reports on the Progress of Chemistry, Section C (Physical Chemistry)*, 106:77–100.

Sunagawa, I. (2005). *Crystals*. Cambridge University Press.

Tanaka, R., Sakemoto, R., and Ohmura, R. (2009). Crystal growth of clathrate hydrates formed at the interface of liquid water and gaseous methane, ethane, or propane: Variations in crystal morphology. *Crystal Growth and Design*, 9:2529–2536.

Tohidi, B., Burgass, R., Danesh, A., Ostergaard, K., and Todd, A. (2000). Improving the accuracy of gas hydrate dissociation point measurements. *Annals of the New York Academy of Sciences*, 912(1):924–931.

Torres, R. E. (2015). Directional solidication of methane hydrates with controlled crystal growth velocities. Undergraduate thesis, Universidad de los Andes & Royal Military College of Canada, Kingston, ON, Canada.

Uchida, T. and Kawabata, J. (1996). Measurements of mechanical properties of the liquid co_2 -water-hydrate system. *Energy*, 22:357–361.

Uchida, T., Moriwaki, M., Takeya, S., Ikeda, I. Y., Ohmura, R., Nagao, J., Minagawa, H., Ebinuma, T., Narita, H., Gohara, K., and Mae, S. (2004). Two-step formation of methane-propane mixed gas hydrates in a batch-type reactor. *AIChE Journal*, 50(2):518–523.

Ueno, H., Akiba, H., Akatsu, S., and Ohmura, R. (2015). Crystal growth of clathrate hydrates formed with methane + carbon dioxide mixed gas at the gas/liquid interface and in liquid water. *New Journal of Chemistry*, 39:8254–8262.

Vysniauskas, A. and Bishnoi, P. R. (1983). A kinetic study of methane hydrate formation. *Chemical Engineering Science*, 38:1061–1972.

Wu, H.-J. and Englezos, P. (2006). Inhibiting effect of triethylene glycol and glycerol on gas hydrate formation conditions. *Journal of Chemical & Engineering Data*, 51(5):1811–1813.

Zhang, Y., Debenedetti, P. G., Prudhomm, R. K., and Pethica, B. A. (2004). Differential scanning calorimetry studies of clathrate hydrate formation. *The Journal of Physical Chemistry B*, 108(43):16717–16722.